DELFT UNIVERSITY OF TECHNOLOGY

Development of Cell to System Annual Energy Yield Toolbox for Bifacial Modules

by

E. Garcia Goma

(4516060)

A report submitted in partial fulfillment of the SET3901 Graduation Project course of the MSc Sustainable Energy Technology

TU Delft Supervisors: Dr. ir. Olindo Isabella
Dr. ir. Rudi Santbergen
Thesis committee: Prof. dr. ir. Miro Zeman
Dr. ir. Milos Cvetkovic

April 2018

DELFT UNIVERSITY OF TECHNOLOGY

Abstract

Development of Cell to System Annual Energy Yield Toolbox for Bifacial Modules

by E. Garcia Goma
(4516060)

Accurate Annual Energy Yield (AEY) predictions can mean important savings due to optimization of energy generation for both particular and utility scale PV systems. However, currently available commercial modules fall short to faithfully reproduce complex designs, specially involving bifacial modules, where albedo gains are relevant.

This work develops a modular Toolbox for predicting energy yield of bifacial PV modules considering optical effects from the very cell level and accounting in depth for the impact of the surroundings on the performance of the PV panel. A modular or block wise construction has two advantages: it is computationally more efficient and it is handier to implement new blocks or replace current ones without the need of entirely creating a new toolbox. To carry out this goal, the best existing PVMD submodels that can fit within the Toolbox are determined, the missing sub-models or pieces within the Toolbox are developed and finally all the parts are integrated and an accuracy assessment carried out. Finally, the Toolbox is applied to optimize the design for a real case of a floating PV structure.

Contents

List of Figures

Chapter 1

General Introduction

1.1 Status of bifacial photovoltaic technology

Since the invention of the first photovoltaic (PV) device by Edmond Becquerel in 1839 [9], which allowed to generate electrical power directly from the incoming solar radiation, many have contributed to the optimization, development and implementation of such devices. In 1883, Charles Fritts developed the first solar cells, being wafer based semiconductor PV devices, in this case Selenium. Afterwards, in 1941, Russel Ohl patented the first p-n junction solar cell [10], which is based on two joint blocks of a single semiconductor material, in this case Silicon, which contain excessive number of electrons (n-type) or excessive number of holes (p-type). The same laboratory, in 1954, achieved crystalline-Silicon (c-Si) PV devices with an efficiency of 5-6 % [11]. This marked the start of large scale deployment of PV devices, based mostly on Silicon, due to its stability, non-toxicity, abundance, and existing extensive research of their physical properties [12].

During the last decades, several concepts that focus in a better separation and management of carriers within the cell, such as heterojunction technology (HJT) and passivated emitter rear contact (PERC), have improved the efficiency of single junction c-Si solar cells, reaching 26.6% efficiency for the first one and 25.3% for the latter [13]. These values come extremely close to the theoretical efficiency limit of single junction c-Si solar cells of 32% established by Shockley-Queisser [14]. It is for this reason that novel approaches to improve efficiency and that go beyond the traditional concepts of reducing recombination are gaining popularity in the recent years. For instance, multi-junction cells (MJ) [15] for a better light management, inter-digitated back contacted (IBC) cells for a reduced shading and bifacial cells, which can efficiently convert light received from

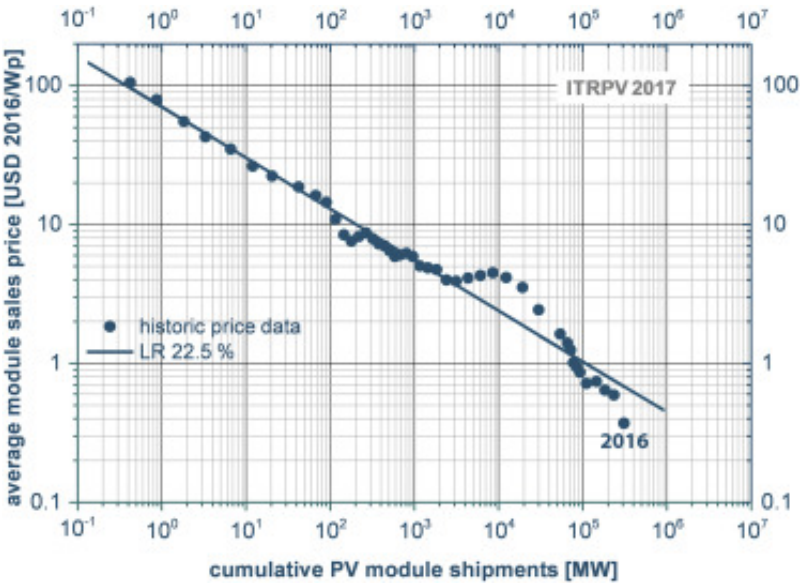

FIGURE 1.1: Learning curve for PV modules, as taken from [1]

both sides while using the same mounting surface, are on this list. It has to be noted that these concepts are not exclusive and can be applied simultaneously.

Commercially, solar cells have been traditionally arranged into 60 cell solar modules, which represent a sweet spot between size, weight and generated voltage. This devices are sold based on their Watt peak (Wp) capacity, meaning the electrical power that they can generate under standard tests conditions (STC). It has to be noted that when arranged in modules, the efficiency of the PV device is reduced in a range of 2% to 3% absolute due to current mismatch between cells and resistive losses, among others [16]. Figure 1.1 shows the decreasing cost trend of PV modules due to scaling during the last years as a function of manufactured capacity. The reason behind this large cumulative PV module deployment is initially the German Feed-in-Tariffs during the 90's and later on the Chinese manufacturing capacity. Altogether, this has led to an extremely competitive market where the cost of the PV module plays a ever more reduced role in the total balance of system (BoS) cost of the PV system [17], which includes inverter, wiring, and mounting costs, among others. Therefore, the aforementioned approaches to enhance efficiency without having an impact on the BoS are on the spotlight now.

Recent cooperation between research institutes and industry, have succesfully achieved the goal of producing commercially available and high efficient bifacial and IBC n-type c-Si PV modules without representing a significant cost in terms of modification of current production lines, with efficiency of 20.4% and 22%, respectively [18, 19]. It has to be noted, however, that bifacial modules are currently rated based on their front performance, and therefore a gain of i.e. 20% in current due to rear generation would boost the efficiency of the aforementioned module up to 24.5%. As a consequence,

bifacial modules are nowadays one of the technologies with greater growth expectations and are expected to represent 25% of the PV market share in 10 years [17]. This is backed up by the recent installation of large bifacial PV farms, being the largest of 50 MWp in China and of 0.4 MWp in Europe [20].

1.2 Relevance of photovoltaic modelling and simulation

Bifacial modules, as well as other innovative photovoltaic concepts that have been developed in the past and that have enhanced the efficiency and deployment of solar technology, have not only been consequence of experimental research. An extremely important catalyzer of such developments is computer modelling and simulation, which is the art of digitally reproducing the key parameters that affect the performance of photovoltaic devices and the interaction between them. In this way, the need of creating a physical prototype is minimized to solely validation goals and final commercial devices. Besides the obvious material cost saving, there is also an important time saving. A model does not only allow to save manufacturing and testing time of prototype, but it is able to perform millions of calculations per seconds, thanks to computational advancements, and thus solve optimization problems in short periods of time.

Traditionally, photovoltaic models can be of two types, mechanistic or theoretical. Mechanistic models are based on empirical data and then the development of equations that fit into this data. This is possible to do [21], however it requires extremely large amounts of data and time, as well as it does not provide scientific proof that it can be employed in other locations or setups than the ones already studied.

On the other hand, theoretical models, are divided in three sub-models, optical, thermal and electrical. The combination of the three of them allows to predict electrical output from the photovoltaic device based in input parameters such as weather conditions, location and electrical parameters or structure of the photovoltaic device. Since modelling is based in the mathematical interpretation of a natural occurring phenomenon, several approaches can be used for the same sub-model. Generally speaking, the more relevant parameters a sub-model comprises, the more accurate will be the results obtained compared to real life values. However, it has to be noted that the more computational operations a model or sub-model performs, the more time-consuming it becomes. Therefore, a trade-off between accurateness and modelling time is sought by developers. Finally, the combination of different sub-models in a single package is the common approach used by developers, in order to provide a turn-key program for end users. This opens the door to several combinations that lead to the multiple amount of model packages found in the literature, each of them featuring its own advantages and short-comes.

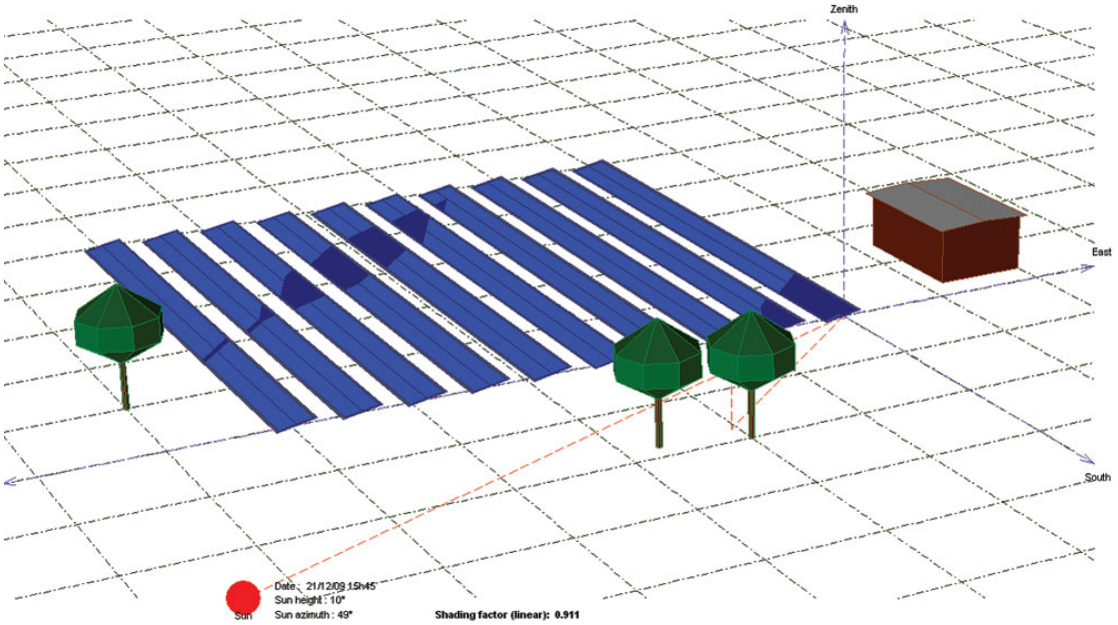

FIGURE 1.2: Screenshot of the PVsyst interface showing the three dimensional model that is employed to analyse shading losses [2]

One common and well-known example of turn-key commercial software is PVsyst [22]. This software can provide a initial estimate of the expected hourly energy yield based on the location meteorological data, as well as a detailed planning on the orientation and sizing of the BoS components. This software, however, uses certain assumptions in terms of calculating shading losses or bifacial gains that can induce into error. For instance, shading losses are calculated based on the amount of corners shaded per every module string, meaning groups of 16 to 22 cells, and not per every individual cell [23]. Figure 1.2 shows a design build in PVsyst and how the shade are reproduced, this is, building the surroundings in a three dimensional model. Regarding bifacial gain, PVSyst also makes relevant assumptions [24]. Firstly, it assumes that the light reflected from the ground is isotropically distributed at all times, multiplied by a fix albedo factor, therefore neglecting different surface reflecting distributions and the fact that albedo varies depending on the time of the day [25]. Afterwards, it weights this irradiance multiplied per the bifaciality factor, which is the ratio between rear and front efficiency performance under STC, and adds it to the front irradiance. Therefore it does not account for three important factors. Firstly, that the light reflected on the rear side is not uniform, and therefore current mismatch occurs. Secondly, that simultaneous illumination performance is not always fully extrapolable from rear and front side performance measured separately, as it depends on the module architecture [26]. Finally, the fact that bifaciality coefficient is not perfectly constant among irradiance and it can vary 1 to 2% absolute [26] makes the model less accurate at low irradiance levels.

Other known PV module level energy prediction models are PV F-Chart [27] and the

System Advisor Model (SAM) by NREL [28]. Both models use meteorological and location data and employ as well their own optical, electrical and thermal models. However they still have shortcomings, specially refering to the optical part. PV F-chart does not have the ability to perform shading analysis. SAM, on the other hand, does perform shade analysis but in a very similar way as PVsyst, this is, building your own three dimensional setup step by step. This is an inconvenient since it requires a lot of time and the necessity of exactly knowing the distance between relevant objects close to the module.

It has to be noted, however, that the aforementioned models only provide information at a module level, and therefore the electrical characteristics of the module under analysis at STC need to be included as an input. For a lower level analysis, other software, such as SmartCalc.CTM, has to be used to bridge the gap [29]. This is a software that evaluates the cell to module optical and electrical losses. Besides, it is worth noting that none of the aforementioned software provide the possibility of modeling curved PV modules, which play an important role in applications such as building integrated PV (BIPV).

To this point, it is clear that modelling is an extremely useful part of PV science, which if applied correctly, can mean important savings due to optimization of energy generation for both particular and utility scale PV systems. However, currently available commercial modules fall short to faithfully reproduce complex situations, specially involving relevant shading and bifacial modules, as well as a turn-key model that is able to perform annual energy ratings starting from the cell level. This issues, which might have not been crucial in the past, become more and more relevant nowadays because of three main reasons.

Firstly, the reduction in cost of PV devices expands the market of non-traditional architecture PV modules, for instance flexible and bifacial PV modules, which in the past represented a negligible percentage of the total. These type of modules require an optical modelling that is able to accurately predict direct, diffuse and surrounding reflected light, taking into account all the parameters that might influence this values.

Secondly, this expansion of PV devices also involve a higher amount of capacity being installed in not so common applications, such as BIPV, which require an excellent and preferably fast shading analysis, or floating PV, as shown in Figure, which demands new features like assessment of water effect on module temperature.

Finally, and also linked to this reduction on price, developing countries are blossoming in terms of PV interest and installations. Developing countries, however, have very different climate conditions from European countries, which mainly dominated the market. This

FIGURE 1.3: Example of a recently blossoming architecture PV module, bifacial PV; fulfilling a new application, floating PV; in a non-European location, China [3]

means that not only orientation should be taken into account when designing PV systems for those modules, but also an assessment on what type of cell technology better suits such conditions also needs to be provided. It is for this reason that a comprehensive model that goes from cell to annual energy yield level is required.

1.3 Goals of this Thesis within the PVMD and PV community

Therefore, it is of the interest of photovoltaic world in general to develop a comprehensive cell to annual energy yield model that can tackle the aforementioned issues and provide an accurate energy prediction for situations such as the one shown in Figure 1.3.

1.3.1 Goal 1: To build a modular AEY bifacial toolbox

The goal of this work is to develop a modular Toolbox for predicting energy yield of bifacial PV modules considering optical effects from the very cell level and accounting in depth for the impact of the surroundings on the performance of the PV panel. A modular or block wise construction has two advantages: it is computationally more

efficient and it is handier to implement new blocks or replace current ones without the need of entirely creating a new toolbox. The subgoals are determining the best existing PVMD submodels that can fit within the Toolbox, to develop the missing sub-models or pieces and finally to integrate all the parts and carry out an accuracy assessment. This goal and subgoals are listed below:

- Goal 1: To build a modular AEY bifacial toolbox:
  - Subgoal 1.1: Identify best match of PVMD models.
  - Subgoal 1.2: Develop missing pieces.
  - Subgoal 1.3: Integrate and assess accuracy.

1.3.2 Goal 2: To apply it to optimize design of a real case

As a second goal, the Toolbox is applied to optimize the design for a real case of floating PV device. The optimum module design for such specific application and location is determined. The main considerations for choosing the case analysis are that such case can benefit from the main advantages of the Toolbox compared to traditional commercial software, such as the ability to reproduce complex designs, the capacity to account for angle of incidence and spectral effects, and the careful consideration of the albedo component. This goal and subgoals are listed below:

- Goal 2: To optimize design of a real floating PV case:
  - Subgoal 2.1: Account for angle of incidence and spectral effects.
  - Subgoal 2.2: Reproduce complex design.
  - Subgoal 2.3: Account for bifaciality and albedo gains.

Chapter 2

Toolbox Approach, Model Review and Case Analysis Introduction

The present chapter firstly analyzes in depth which are the parameters that are relevant to such model. In the same section, the submodels existing literature, both commercial and scientific, are studied in order to identify the critical sections that need to be improved. The most relevant PVMD and external literature models are analyzed in this chapter and the most suited ones are selected to be implemented later in the toolbox with or without further modification. Additionally, a look into what integration tools are required to put together all the submodels is given as well.

For the optical part of such model, which comprises the Cell Technology Block, the System Setup block and the Sky part of the Location Integration block, the Photovoltaic Materials and Devices (PVMD) group from the Technical University of Delft has developed separated tools that can approach some of the concerns individually. For instance, the GenPro4 software developed by Dr. R. Santbergen can provide a comprehensive optical analysis at cell level, while the LUX software provides an environment to scale up this optical analysis to module level, providing an accurate shading and albedo analysis related to elements close to the module. From this environment, a sensitivity map can be coupled with a Sky Map obtained from meteorological database, tecnique optimized by V. Muthukumar. It is worth noting, however, that these tools have been originally developed for monofacial modules, and thus a further section of the present thesis is dedicated to the adaptation of the aforementioned models into bifacial ready codes.

Regarding electrical and thermal models, standard approaches will be reviewed and used. This section will also include an analysis on how water floating devices have their temperature influenced and how to make a model that satisfactorily reproduces such

effects. Afterwards, other relevant issues such as losses due to long term degradation induced, for example by light (LID), are discussed.

Finally, a detailed study case is introduced. This case is based on floating PV panels on water canals in the Netherlands, under the INNOZOWA project granted by the Dutch Government.

2.1 Toolbox Composition

For clarity reasons and highlighting its most relevant features, it is called "Cell to System Annual Energy Yield Toolbox for Bifacial Modules". For the sake of conciseness, however, along this report this Toolbox might be referred to simply as the 'Toolbox'. In this section the layout of the Toolbox and the integration methods are discussed.

2.1.1 Decomposition of space

One of the main characteristics of the Toolbox, as described in the goal section, is that it shall be modular. Therefore a modular layout for it shall be designed. As a first step towards this design, the reality to simulate shall be described. Figure 2.1 shows an example of a bifacial PV roof installation. This sample situation can be split in three units in which the simulation output carried out at each unit can be independent of the following ones: Cell, System Setup and Location. For instance, the reflectivity of a cell is independent of the setup or location in which is placed, whereas the relative ability of a setup to absorb light incident from a certain direction is independent of the location in which it is placed. Figure 2.2 and 2.3 graphically present this concept.

2.1.2 Toolbox layout

Based on the previous space decomposition, the Toolbox can be divided in three blocks: the Cell Technology Block, the System Setup Block and the Location Integration Block.

The Cell Technology Block and the System Setup Block aim to determine the optical properties at cell level and at module level, respectively. These can be used to optimize parameters such as cell layer thickness and module tilt for a certain location, for example. Regarding the Location Integration Block, it includes optical, thermal and electrical parts. Figure 2.4 shows the layout of the Toolbox. The input for the Cell Technology Block are the cell layer properties, such as material, thickness and texture, whereas the output is the optical absorption, reflection and transmission of the entire cell, as a

FIGURE 2.1: Example of a bifacial PV installation on a roof [4]

FIGURE 2.2: Example of a bifacial PV installation on a roof, where the space is separated in three units: Cell (orange), System Setup (blue) and Location.

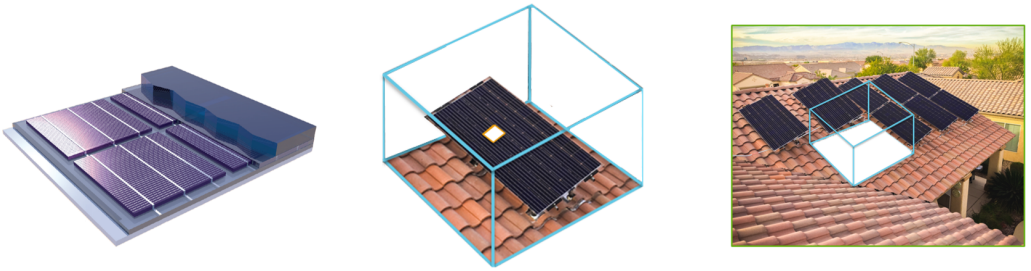

FIGURE 2.3: Decomposition of the three units in which space is separated: Cell (left), System Setup (center) and Location.

function of wavelength and angle of incidence (AOI). The absorption at the c-Si layer, responsible of generating the current, shall also be assessed. For the System Setup Block, the input shall be the geometrical design and optical properties of the setup, together with the output of the Cell Technology Block. The output shall be an assessment of how much light is absorbed by the c-Si layer as a function of its incident direction, also known as Sensitivity. For the Location Integration Block the input shall be the Sensitivity and the Meteorological data, together with relevant PV module electrical parameters information which can be extracted from the datasheet. Its final output is the DC Annual Energy Yield (AEY) for the given cell technology, in such a setup, for the specific location and time period from which the meteorological data is retrieved.

2.1.3 Integration tools

Due to the large amount of mathematical models that have to be run together, a programming language shall be employed when integrating them into a single toolbox. Most of the programs within the PVMD that exploit such models are written in either Matlab or Phyton, therefore one of these two is employed when developing the toolbox. It is to be noted, however, that one of the most elaborated models that will be employed, the GenPro4 and LUX, as discussed in the next sections, are based in Matlab and thus employing this environment for building up the rest of the toolbox will optimize the research carried out.

2.2 Cell Technology Block review and analysis

The energy generated by a PV system is primarily consequence of the photoelectric effect carried out by solar cells, when light is absorbed by it. This absorption is proportional to the irradiance incident on the surface of the cell, and the way it interacts with each layer of the cell structure. The study and modelling of the light interaction at cell level

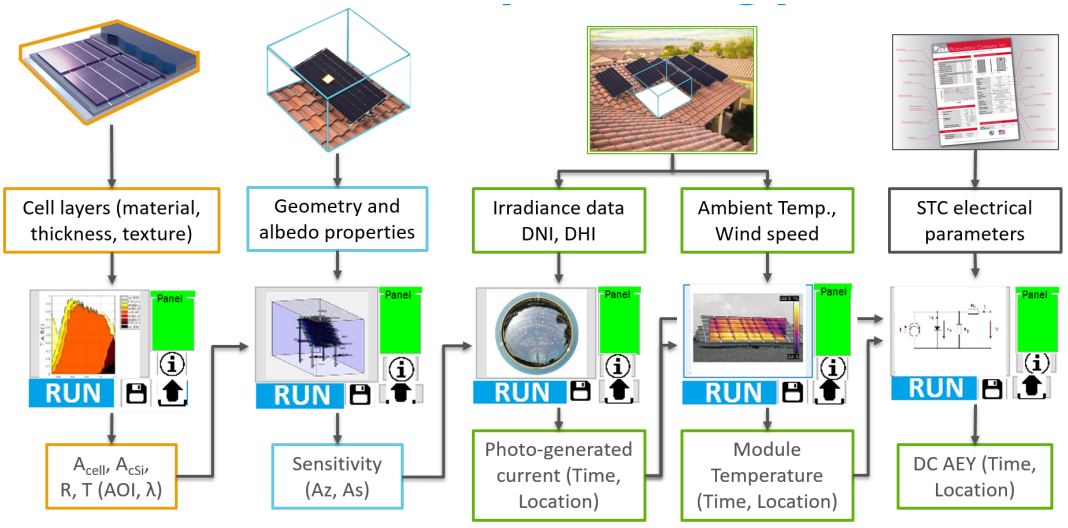

FIGURE 2.4: Toolbox layout, including input and output, based on the space decomposition shown in Figure 2.3. Parts corresponding to Cell Technology, System Setup and Location Integration Block are shown in orange, blue and green, respectively.

is comprised in this project in the so called Cell Technology Block. Conceptually, a solar cell is a device formed by different layers stacked on top of each other. Depending on the thickness a layer, the full electromagnetic wave behaviour of light plays an important role in the way light interacts, since it takes into account effects such as diffraction [30]. This happens for layers with sub-wavelength thicknesses. For thicker layers, on the other hand, light interaction can be well described with ray-tracing models. In this case, it is assumed that light travels without interference through the bulk of each layer. In the interlayers and external surfaces, however, reflection, transmission, or a balance of both, either in scattered, specular or combined way, might occur. In general, the inputs required in such models are the characteristics of each layer, including thickness, roughness, refractive index and extinction coefficient.

Most of the optical models found in literature are based in wave optics or ray optics [30]. While they all present of course conceptual similarities, modelling optimization plays a key role in order to achieve a fast computational time while having highly accurate results. Looking at the big picture of the project, and since the Cell Technology Block is a block in one of the sections of the whole toolbox, a fast computational time is indeed a crucial feature. Research carried out by Santbergen et al. [30], reviews the optical models with these characteristics published up to date, and proposes an improvement of its own model [31], applicable both for thin film and wafer based cells, with an excellent trade off of time and accuracy and easily tunable if even quicker simulation times were desired. As input, an atomic force microscopy (AFM) scan can be used, the comprehensive nature of which will set the base for accurate results. On the other hand,

the reflection, transmission and absorption as a function of wavelength for the solar cell as a whole can be extracted as output. For these reasons this model is chosen as the base of the Cell Technology Block of the optical model of the toolbox. It has to be taken into account, however, that the model at the present time is limited to simulate layers, therefore parts of the cell that fall out of this definition, such as metallic fingers, are omitted.

It has to be noted that this model, as well as the rest of optical models reviewed in the aforementioned paper, are designed to operate with a single light source, meaning they lack the feature of simultaneously simulate front and rear irradiation, situation which is relevant for bifacial cells. A simple way of overcoming this challenge, is to perform single light source simulations for a certain solar cell layer structure and, afterwards, perform the same simulation with an inverted layer structure, therefore following a sequential approach. It has to be noted that theoretically, this approach is valid since the front and rear light, as it happens in outdoor conditions, are independent and not coherent, since after reflection or scattering, all the correlation that front and rear light might held is lost. Therefore they do not interfere with each other and a sequential approach is feasible.

2.3 System Setup Block review and analysis

Once the raw cell values of absorptance, reflection and transmission as a function of angle of incidence have been determined, the solar cell can be simplified to a single object. In this way, bigger scale ray tracing can be easily designed and computed. The first step is to spatially arrange the cells module-wise, leaving certain intercell spacing between them, as it would be for a typical commercial module. Then, the encapsulation layer, as a single object, has to be placed surrounding the cells in all directions, filling the intercell space. Afterwards, the glass or backsheet front and rear layers have to be included on top or bottom of the encapsulation object. Finally, if the device to be designed features it, a frame shall be included at the edges. Once the whole module is modelled, the surroundings have to be designed, with the same program. All the relatively close objects that reflect a relevant amount of light or that cast shade on the module shall be considered. This generally includes mounting frames, surface below the structure and neighbouring modules. After the setup is built, the relative incident amount of light over each cell at any given irradiance condition shall be calculated. This relative light map is the so called sensitivity map [32]. An in house software developed by R. Santbergen called Lux allows to construct the desired structure inside a cube and have a sort of infinite map by making the rays that exit the cube appear in the opposite

side. This is extremely useful to characterize for instance solar modules that are found in the middle of an array on a PV farm, whitout having to also model the rest of modules in the row. Commercial softwares that perform ray-tracing are also available, for instance LightTools. However such software does not allow to perform the infinite map that Lux features.

2.4 Location Integration Block review and analysis

These blocks aims to integrate the location independent blocks such as Cell Technology Block and System Setup Block with the meteorological data of the location in order to assess the module and c-Si layer irradiance absorption as well as the cell temperature and in consequence the final DC power generation.

2.4.1 Sky Model

The Sky Model forms the first part of the Location Integration block. This part considers the percentage of direct normal irradiance (DNI) and diffuse horizontal irradiance (DHI) at a given time for a given location, and its absorption by the PV module. Using a decomposition model, the DNI and DHI at a given time can be represented in the so called Sky Map, where the amount of irradiance is presented per direction of incident light, this is as a function of azimuth and altitude. Traditional approach for Sky Map, like the one used by V. A. Muthukumar based on the Perez model [32] effectively combines the position of the sun with meteorological data, from sources such as Meteonorm, in order to obtain the base Sky Map.

Furthermore, to take into consideration the shading caused by buildings, a principle like the horicatcher can be used. This principle can be added to the base skymap and deduct certain amount of light that will not reach the module due to neighbouring structures. In order to do so, two different approaches can be employed. One one hand, ray tracing, as discussed earlier, is suitable for this sort of macro analysis. On the other hand, it can also be used the so-called vector algebra approach, which is characterized by its short computational time.Regarding the vector algebra approach, it consists of a projection of the surroundings over the module surface, in order to understand how much shading is casting over it, avoiding the time consuming act of tracing every ray. This approach has been successfully employed by G. Faturrochman [33] on bifacial modules, providing accurate validated results. In this work both ray tracing and vector algebra approaches are considered.

Finally, for accounting transient shade effects, recent work by Ziar et al. [34] has demonstrated that if not accounted, can generate losses due to partial shading of the modules, not accounted for in traditional models.

2.4.2 Thermal Model

The performance of PV module relies highly on the temperature at which the device operates. This is mainly consequence of the recombination effects that occur in the junction layer and the rates at which they take place, which vary at different temperatures. Such is the importance of the module operating temperature that it is mandatory for manufacturers to report, on top of the performance at STC, the Normal Module Operating Temperature (NMOT) performance, which is an updated term of the Nominal Operating Cell Temperature (NOCT) [35], of their solar modules in the datasheet to which the customer has access. The NMOT, however, is defined at certain meteorological conditions which are a wind speed of 1 m/s, an ambient temperature of 20 C and an irradiance of 800 W/m^2. These conditions, however, do not always hold true for different locations, seasons or even time of the day. Therefore it is of vital importance to determine the operating temperature of a PV device during every single period of time: the shortest the period, the most accurately can the performance be determined.

2.4.2.1 Relevant parameters for defining operating temperature

As seen in the previous paragraph, meteorological conditions play an important role when defining the operating temperature of PV devices. Besides, the mounting structure and the power flowing through the device also affect this temperature.

Regarding meterological conditions, the most relevant are the irradiance falling into the solar panel, and its angle of incidence, since this will affect the amount of light it is actually absorbed in the solar device and which by extension will determine its rate of thermalization and infrared light absorption, which both heat up the device. Other parameters are the ambient temperature and the wind speed, which will change the device temperature due to convection effects.

The mounting of the PV module will also affect the temperature since it can create inhomogeneity in the manner that wind flows over the surface and back of the PV device and also due to one end being closer to the ground for tilted modules, which will create a gradient in the temperature of the PV device.

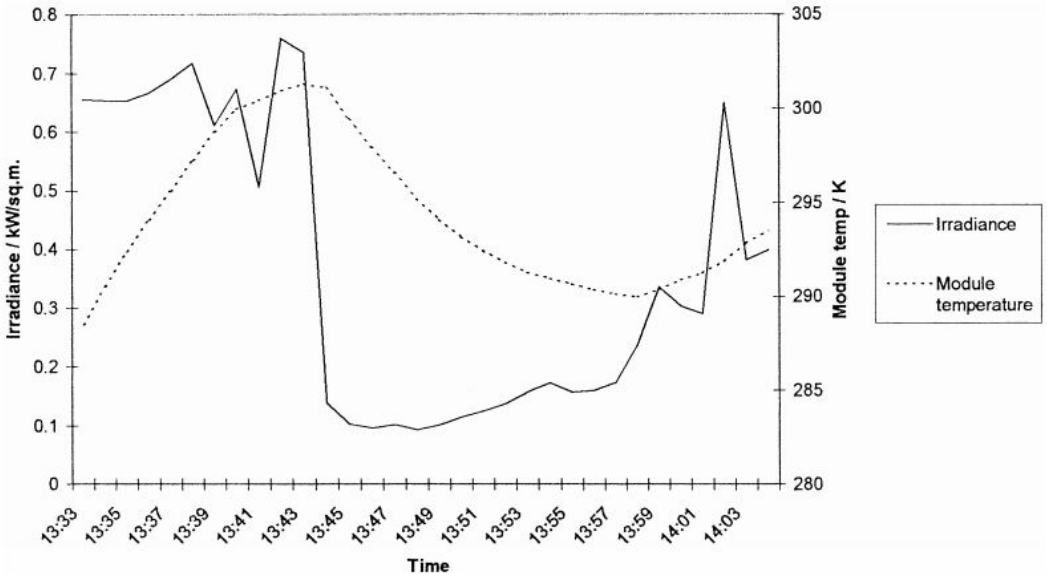

FIGURE 2.5: Module temperature response to rapid step change in irradiance corresponding to data from 3/2/96 for a module mounted facing South in Newcastle Upon Tyne, UK, and taken from [5]

Finally, the power flow that the PV device is generating also plays a relevant role in the temperature due to obvious reasons, since if more power is retrieved from the device, less power has the possibility to be converted into heat.

2.4.2.2 Dynamics and rapidness of temperature changes

As in any single empirical process in nature, the variations in temperature of a photovoltaic device do not occur instantly but require certain response time. This consideration is specially relevant in rapidly fluctuating climate conditions, as shown by [5] in Figure 2.5.

Based on this premise, thermal modules can be classified in two bins, Steady-State models, and non-Steady State models. The time constant of a PV module is the time that it takes for it to reach 63% of its final temperature [5]. Normally this time constant is around 7 minutes [36]. Therefore for datasets that involve input with a time separation above 7 minutes, like it will be in the model presented in this Thesis since it aims to annual energy yield studies, with hourly or 10 minutes input, it is convenient to apply Steady State models.

2.4.2.3 The NMOT model and its variations

An example of Steady State model is the model based on NMOT provided by Stultz [35], adapted and described by Equation (2.1), which only takes irradiance G_M, ambient temperature T_a and the manufacturer datasheet value of NMOT as input. This model is based on the assumption that the difference between module and ambient temperature changes linearly with irradiance, using as a reference point the NMOT conditions of 20 C and 800 W/m$_2$. Due to its simplicity and low amount of input parameters required, this model is still used when limited meteorological input values are available [37].

$$T_M = T_a + \frac{T_{NMOT} - 20}{800} * G_M \tag{2.1}$$

It is to be noted that evolved versions of this Steady-State model have been developed, such as the Duffie-Beckmann model [38], which takes into account the energy balance of all the irradiance incident on the solar panel G_{POA}, breaking it down between that that is extracted as power output and that which is converted into heat, as shown in Equation (2.2), where τ and α are transmittance and absorbance of the module, respectively, μ_m is the efficiency of the module, and U_L is the heat losses due to convection, conduction and radiation.

$$(\tau\alpha)G_{POA} = \mu_m G_{POA} + U_L(T_{cell} - T_{amb}) \tag{2.2}$$

Using the values at NMOT and combining it with Equation (2.1), Equation (2.2) can be expressed as (2.3), derived by Jamokdar [39]. Values for U_L and U_{LNMOT} can be found in literature [38].

$$T_{cell} = T_{amb} + \frac{G_{POA}}{800}(\frac{U_{L,NMOT}}{U_L})\frac{T_{NMOT} - 20}{800}(1 - \frac{\mu_m}{\tau\alpha}) \tag{2.3}$$

2.4.2.4 The fluid-dynamics model and its variations

A more comprehensive thermal model that elaborates a detailed energy balance between the PV device and its surroundings is the fluid dynamics model. Because of its in depth energy analysis, it takes as input parameters all sorts of parameters such as cloud

coverage and ground temperature, among others. One of the pioneers in such models is the one developed by Fuentes et al. [40], thoroughly summarized by Isabella et al. [36] and validated for Delft environment by Jamodkar [39].

This model assumes that the module is a single uniform mass at temperature T_m, determined by heat exchange with the environment by conduction, proportional to the irradiance received from the Sun G_M and determined by the absorptivity α of the module; convection with the air for the front and rear side; and radiation between the front side of the module and the sky. T_m can be described as in the following Equation (2.4).

$$mc\frac{dT_M}{dT} = \alpha G_M - h_c(T_M - t_a) - \epsilon_{back}\sigma({T^4}_M - T_{4gr}) - \epsilon_{top}\sigma({T^4}_M - {T^4}_{sky}) \quad (2.4)$$

Where the first term to the right of the equal sign signifies the conduction heat, the second term the convection heat losses and the last two terms the radiative losses for front and rear. The radiative part can be simplified and made linear to T_M via Equation (2.5) and (2.6).

$$h_{r,sky} = \epsilon_{top}\sigma({T^2}_M + {T^2}_{sky})(T_M + T_{sky}) \quad (2.5)$$

$$h_{r,gr} = \epsilon_{back}\sigma({T^2}_M + {T^2}_{gr})(T_M + T_{gr}) \quad (2.6)$$

Substituting in Equation (2.4) and equalizing to zero Equation (2.7) is obtained.

$$\alpha G_M - h_c(T_M - T_a) - h_{r,gr}(T_M - T_{gr}) - h_{r,sky}(T_M - T_{sky}) = 0 \quad (2.7)$$

Which rearranging leads to Equation (2.8).

$$T_M = \frac{\alpha G_M + h_c T_a + h_{r,gr}T_{gr} + h_{r,sky}T_{sky}}{h_c + h_{r,gr} + h_{r,sky}} \quad (2.8)$$

Detailed calculations on how to find the convective heat transfer h_c can be found in [36].

Finally this model has also been adapted to Bifacial PV modules by [41] and validated for Netherlands environment by Faturrochman et al. [42].

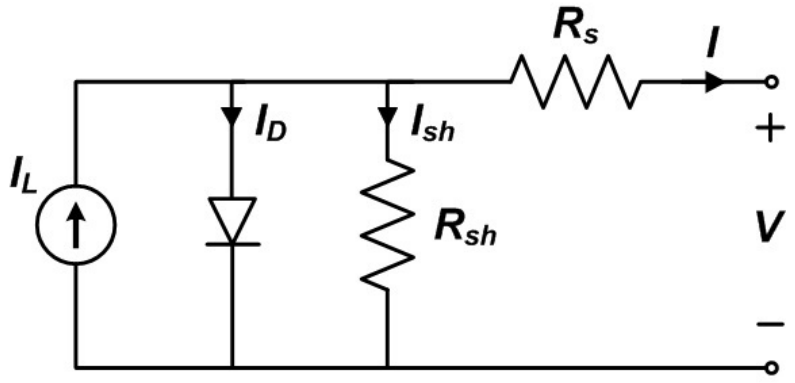

FIGURE 2.6: Equivalent circuit of a solar cell

2.4.3 Electrical Model

Although PV panels are a pleasant sight, aesthetics is not their main purpose, but the generation of electricity. So far this chapter has covered the literature related to the absorption of light and creation of electron-holes pairs. It is now the turn for this electrons and holes to be carried successfully to the metal contacts of the PV device, thus generating direct current (DC) power. And that, of course, can be modelled.

2.4.3.1 The equivalent circuit of a solar cell

The DC power of a cell depends mainly on four parameters: the short circuit current (I_{SC}) generated, which is proportional to the optical absorption; the open circuit voltage (V_{OC}) between the cell metallic contacts, which is a consequence of its layers characteristics and distribution; and the series (R_S) and shunt resistance (R_{SH}), which will define how much of this current is lost at high voltages, and which also depend of the cell architecture. Said so, the equivalent circuit of the cell can be represented as in Fig. 2.6, where I_L represents the light generated current, I_D represents the current lost due to recombination inside the solar cell and I_{SH} represents the current loss due to shunt resistance. This model is also know as the single-diode model.

Applying the Kirchoff's law, in the single diode model the current flowing through the cell is equal to Equation (2.9). Where I_D is defined using Shockley equation for an ideal diode, shown in Equation(2.10).

$$I = I_L - I_D - I_{SH} \tag{2.9}$$

$$I_D = I_0[exp(\frac{V + IR_S}{nV_T}) - 1] \tag{2.10}$$

where:

I_0 is the saturation current;

n is the ideality factor, which accounts for the recombination effects;

V_T is the thermal voltage.

Now V_T is defined as in Equation (2.11) and R_{SH} as in Equation (2.12). Therefore the total current flowing through the cell is defined as in Equation(2.13).

$$V_T = \frac{kT_C}{q} \tag{2.11}$$

where:

k is Boltzmann's constant ;

T_C is the cell temperature;

q is the elemental charge.

$$R_{SH} = \frac{(V + IR_S)}{R_{SH}} \tag{2.12}$$

$$I = I_L - I_O[exp[\frac{(V + IR_S)}{nV_T}] - 1] - \frac{V + IR_s}{R_{SH}} \tag{2.13}$$

Therefore showing that the single diode model depends on five parameters: I_L, I_0, R_S, R_{SH} and n.

If taken to the module level, for which all the cells are connected in series, the single diode equation takes the form shown in Equation (2.14) [43].

$$I = I_L - I_0[exp[\frac{(V_M + I_M N_S R_S)}{nN_S V_T}] - 1] - \frac{V_M + I_M N_S R_s}{N_S R_{SH}} \tag{2.14}$$

where:

V_M is the module voltage;

I_M is the module current;

N_S is the number of cells in series.

2.4.3.2 The diode constant, photogenerated and saturation current

For the sake of simplicity, some papers reduce the ideality factor n into the modified ideality factor a via Equation (2.15), being n = 1 a perfectly ideal solar cell and taking values between 1 and 2 for most of the practical solar cells.

$$a = N_S n k T_C q \tag{2.15}$$

The value of this constant is to be found empirically and it has to do with the curvature of the IV curve. Several authors such as Vimalarani [44] and Meyer [45] have listed these values for many technologies, as shown in Table 2.4.3.2.

	a-Si:H	Multi-Si	Mono-Si
n	1.71	1.15	1.19

The photogenerated current is directly proportional to the absorbed irradiance such as in Equation (2.16)

$$I_{PV} = (I_{PV,n} + K_I \Delta_T)\frac{G}{G_n} \tag{2.16}$$

where:

K_I is the current temperature coefficient;

As explained in the previous subsection, I_L is directly proportional to the absorbed light irradiance. On the other hand, I_0,which depends on temperature, is defined in a more lengthy manner, as shown in Equation (2.17) [46]. The nominal saturation current ($I_{0,n}$) mentioned in the previous equation is defined by Equation(2.18)

$$I_0 = I_{0,n}(\frac{T_n}{T})^3 exp[\frac{qE_g}{ak}(\frac{1}{T_n} - \frac{1}{T})] \tag{2.17}$$

where:

E_G is the bandgap energy of the semiconductor;
$I_{0,n}$ is the nominal saturation current;

$$I_{0,n} = \frac{I_{SC,n}}{exp(\frac{V_{OC,n}}{aV_{T,n}}) - 1} \tag{2.18}$$

Improvements to the J_O model has been applied by Villalva et al. [46], in order to match the open-circuit voltage to experimental data for large ranges of temperatures, and it is defined as in Equation (2.19)

$$I_0 = \frac{I_{SC,n} + K_I \Delta_T}{exp(\frac{V_{OC,n} + K_V \Delta_T}{aV_T}) - 1} \tag{2.19}$$

where:

K_I is the current temperature coefficient;

K_V is the voltage temperature coefficient;

The main advantage of this approach is that it does not need the E_G of the cells and I_0 can be calculated from parameters provided in the PV module datasheet instead, such as temperature coefficients.

2.4.3.3 Determining series and shunt resistance

Fundamentally, the series resistance of a PV module depends in more factors than just the cell architecture, for instance, in the intercell and junction box connections. Similarly, the shunt resistance, which should be high to avoid current leaving the module through an undesired path, can vary due to manufacturing failures. Therefore, the ideal approach is to find out these values experimentally.
Villalva et al. [46] suggests to extract them from the previously used parameters and the maximum power (P_{MAX}) of the module and its corresponding voltage and current (V_{MP}) and (I_{MP}), as indicated in Equation (2.20) and (2.21).

$$P_{MAX} = V_{MP}[I_{PV} - I_0[exp(\frac{q}{kT}\frac{V_{MP} + R_S I_{MP}}{aN_S}) - 1] - \frac{V_{MP} + R_S I_{MP}}{R_P}) \tag{2.20}$$

$$R_P = V_{MP}(V_{MP}+I_{MP}R_S)/(V_{MP}I_{PV} - V_{MP}I_0[exp(\frac{q}{kT}\frac{V_{MP} + R_S I_{MP}}{aN_S})]+V_{MP}I_0-P_{MAX}) \tag{2.21}$$

Therefore it is shown that per every value of R_S there is its corresponding pair of R_{SH}. The goal is to find the pair of R_S and R_{SH} that make the mathematically calculated P_{MAX} form Equation (2.21) match the experimental Pmax value. This is found by iteration.

It is important to analyze, however, the effect of temperature and irradiance on the values of series and shunt resistance. While it is well known that they are independent of temperature [6], their relation with irradiance is not very straight forward and a quick search in literature can bring confusing insights. Many authors state that their value change with irradiance, such as Eikelboom and Reinders [6], who state that While shunt resistance suffers an exponential decay at higher irradiances, series resistance experiences a reverse exponential increase at higher irradiances, as shown in Figure 2.8 and 2.7. These changes, however, are only apparent, as explained by Reich et al [47], as they represent the differential resistances close to Isc and Voc regions. Apparent series

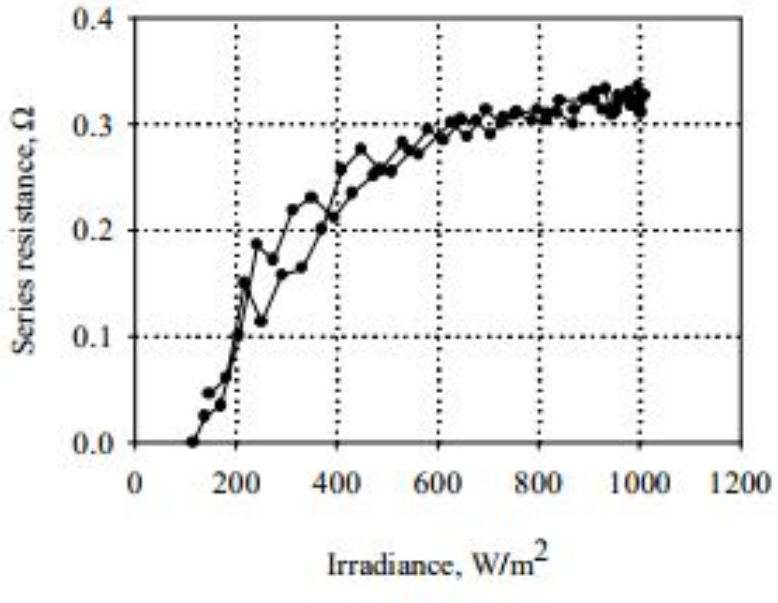

FIGURE 2.7: Series resistance of a samplle solar cell as a function of irradiance [6].

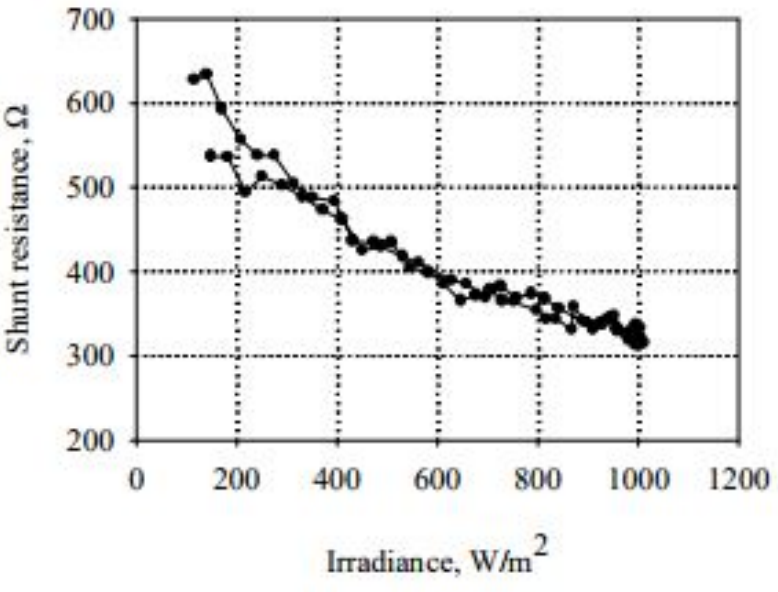

FIGURE 2.8: Shunt resistance of a samplle solar cell as a function of irradiance [6].

resistance represents thus the differential resistance of the clel at Voc and is thus the theoretical upper limit of the real series resistance [47]. Real shunt resistance, on the other hand, is that measured at dark conditions and it converges with apparent shunt resistance at low irradiance conditions.

As a conclusion, the method presented in this subsection calculates the real series and shunt resistance, which is independent of temperature and irradiance.

2.4.4 Prediction of long term performance

As it is well known, solar modules do experience degradation in performance over time when exposed to outdoor conditions. This degradation can have multiple causes, some of them known for long time such as hailing which cracks the cells [48] and ultraviolet degradation of the backsheet [49], and some more recently discovered types such as induced defects due to partial shading of thin films [50] [51], our newly discovered types of light induced degradation on solar cells such as light induced degradation and regeneration at elevated temperatures (LeTiD) [52] [53], among many others.

Because of the massive extent of the concept of degradation on solar modules itself, in this work the degradation in performance of PV panels is neglected. However, the user of this Toolbox must be aware that a degradation similar to the maximum possible degradation conceivable for a solar module according to the manufacturer guarantee in the datasheet might occur over the years for PV panels installed on the field.

2.5 Case study: The INNOZOWA project

The ultimate goal of the model is to serve as a tool to predict the output of different setups in a certain location and consequently choose the optimal one configuration. In order to put this in practice, the framework of the INNOZOWA project has been chosen.

This project is carried out by the TU Delft jointly with other public and private parties from the Neteherlands, and it aims to develop a retractile floating PV system that can be placed in the Dutch canals. The reason behind making them movable is for the maintenance workers to mow twice a year.

In order to provide a small footprint, it is decided to employ bifacial solar panels, which can be placed standing in East-West direction. Note that for an easier withstanding of the wind force, the module shall be standing on the long edge.

Besides, bifacial technology allows to increase the power production of the system by taking advantage of the albedo of the surroundings, therefore generating at least as

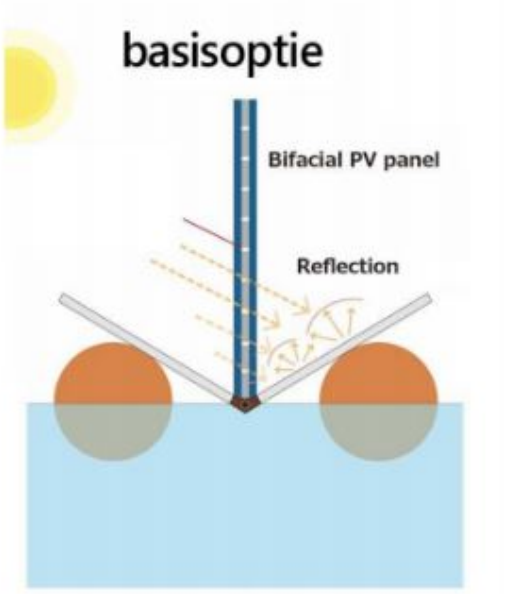

FIGURE 2.9: Design of the prototype of the floating PV system for INNOZOWA project

much energy as a monofacial module placed at an optimum angle. To maximize this advantage, white reflectors placed around the module are considered, as shown in Figure 2.9.

Due to budget constraints, however, the choice of the bifacial module is not fully free, but it is limited to those commercially available in the market. Currently available bifacial manufacturers include LG, Sunpreme and Yingli. From these, LG supplies modules at user scale and thus is selected at this stage.

Besides the PV system, the location plays a great role in the energy yield that can be generated over the year. This is specially important when employing bifacial PV modules. The selected site for the pilot is an artificial lake located in the water treatment plant of Weurt, in the Netherlands, and that is shown in Figure 2.10. Different albedo, shading and wind speed measurements are carried out at the location.

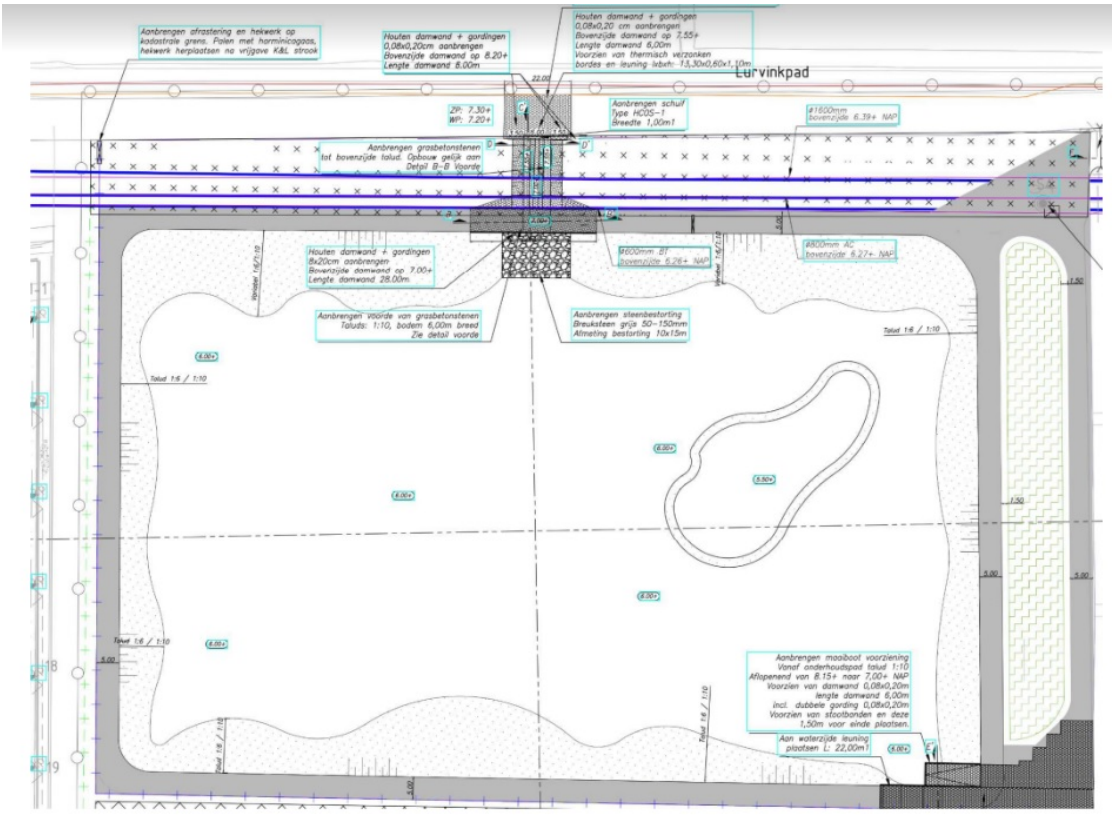

FIGURE 2.10: Top view of the lake chosen for the pilot production in Weurt, The Netherlands

Chapter 3

Cell Technology Block

The goal of the Cell Technology Block is to provide the electrical parameters at STC of the cell technology and its temperature coefficients. This shall be solely achieved by the input of the layer properties of the cell, such as material, thickness and textures. In this way, different cell architectures can be simulated and the toolbox can be employed to optimize architecture for certain mounting or installation location. Alternatively, it shall be possible to input manufacturer datasheet information in case a commercial technology is to be used.

3.1 Concept, input and output

The idea behind the Cell Technology Block is to be able to determine the electrical parameters of a cell or module in order to compare their performance against other technologies or cells of the same technology but with different layer properties.

The input is, therefore the thickness, texturing and composition of the different layers that conform the cell. A cross section of an heterojunction solar cell is shown in Figure 3.1, which also depicts the materials of the layers and their thicknesses. Regarding texture, it is quite common to texture silicon layers in order to increase the light trapping. This texturing can be of many textures although some of them such as pyramids or inverted pyramids, depicted in Figure 3.2, have proven more efficient [54].

The output, in order to be able to perform a full simulation afterwards, shall be the Isc, Voc, Impp and Vmpp at Standard Test Conditions of the solar cell.

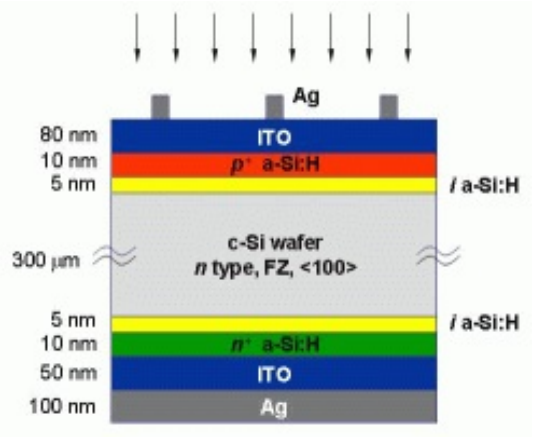

FIGURE 3.1: Cross section of an heterojunction solar cell, showing the thicnkess of the layers and their materials. [7]

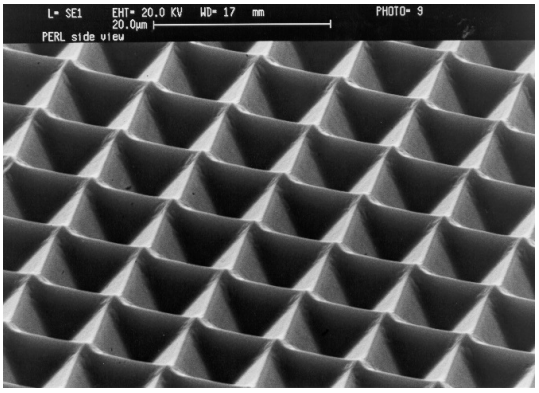

FIGURE 3.2: Textured silicon surface with inverted pyramids, retrieved from [8]

3.2 Possible approaches and algorithms

As discussed in the Chapter 2, the selected approach is to use the optical simulation package GenPro4 in order to understand the light absorption of the cell and by extension its photogenerated current. However, it must be possible for the user to skip this step and be able to input only the manufacturer datasheet information, in case a full characterization of the solar cell is not available. Thus, these two approaches are presented in the following subsections, together with a third extended approach which is also introduced. They are named, respectively, 'Build Your Own Cell', 'Full Datasheet' and 'Build Your Own Cell (extended)'.

3.2.1 Build your own cell

This approach, presented in Figure 3.3, takes advantage of the GenPro4 simulation package to obtain accurate absorption reflection and transmission data of every layer of the cell as a function of angle of incidence and wavelength. This output allows for a more accurate optical absorption analysis afterwards than assuming a constant absorption, reflection and transmission values as it is the regular practice among simulation tools. Furthermore, it is to be noted that despite the absorption of all the layers is provided, the most relevant ones are the absorption on the crystalline silicon layer, since it is directly proportional to the short-circuit current generated by the cell, and the overall absorption value, in order to make a detailed energy balance for thermal calculations.

The input necessary for such calculations are the material of which the layers are build, their thicknesses, and the texturing of those. It is to be noted that EVA and glass layers are also input in this simulation step in order to reduce the simulation load of future blocks that require iteration.

Finally, electrical parameters relevant to an electrical and termal behaviour analsysis are also required, such as open circuit voltage and maximum power under STC, or temperature coefficients. These values must be retrieved either from the manufacturer module datasheet, or from literature values.

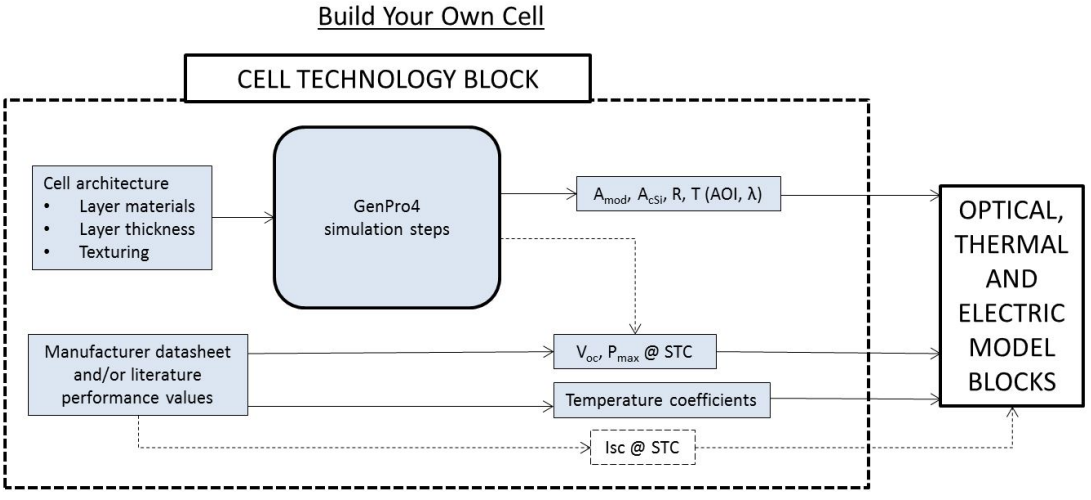

FIGURE 3.3: Algorithm for applying the 'Build Your Own Cell' approach. Dashed paths are not applied in this approach.

3.2.2 Datasheet analysis

Of course, it is well possible that such a detailed input as layer information is not available for all users. Aiming thus to the use of the toolbox by designers or those who have access to less information, the 'Full Datasheet' approach allows to use the Bifacial Toolbox inputting solely information found in the datasheet. Thus, electrical parameters at STC and temperature coefficients are retrieved from this source. This approach is shown in Figure 3.4.

It is to be noted, however, that assuming a sole value of short circuit current prevents from detailed analysis of light absorption at different angle of incidence or under different solar spectrums.

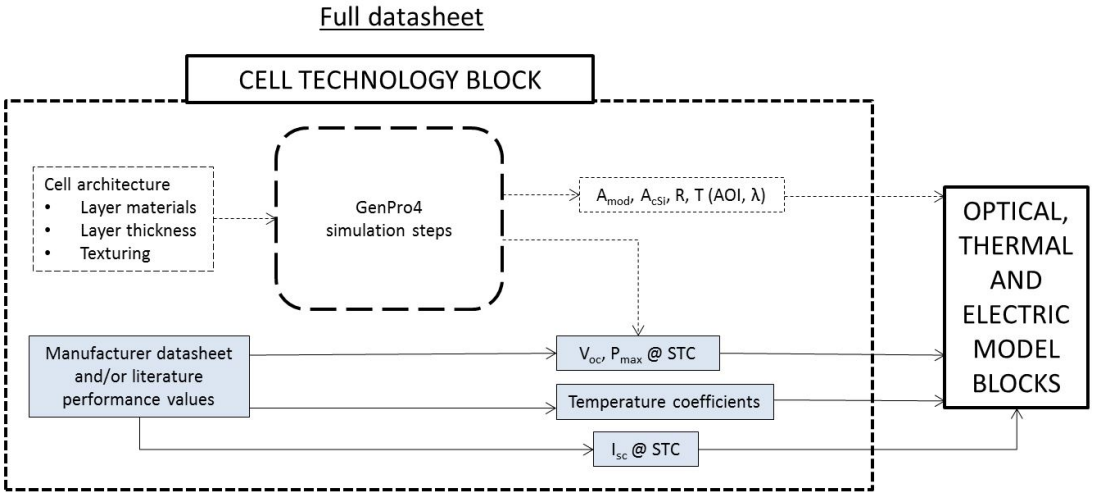

FIGURE 3.4: Algorithm for applying the 'Full Dastaheet' approach. Dashed paths are not applied in this approach.

3.2.3 Build your own cell (extended)

Finally, an approach in which all the electrical parameters are retrieved from the cell architecture, excepts those that are deliverately challenging, such as temperature coefficients, should be possible as well. Such approach is shown in Figure 3.5.

It is to be noted, however, that the tools for such approach are not researched in this work and therefore it is left for future implementations to analyse this method.

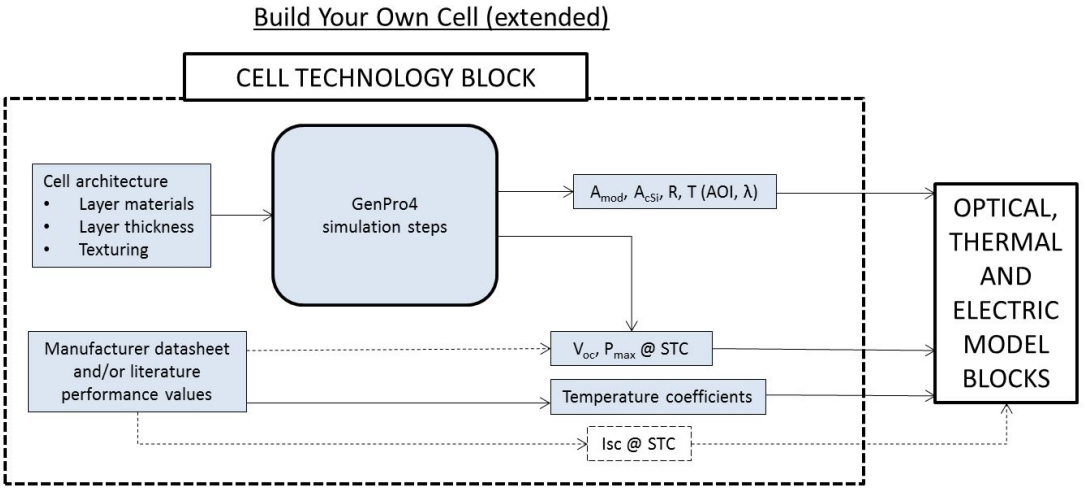

FIGURE 3.5: Algorithm for applying the 'Build Your Own Cell (extended)' approach. Dashed paths are not applied in this approach.

3.3 GenPro4 simulation steps analysis

As discussed in the previous sections, one of the key steps of the 'Build Your Own Cell' approach of the Cell Technology Block passes through a proper usage of the software the GenPro4. This usage requires the input of cell architecture layer preoperties, such as materials, thickness and texture, and the output of c-Si and cell aborption as well as reflection and transmission.

GenPro4, which can operate in different wavelenghts and angle of incidence (AOI), takes all the aforementioned parameters and effects into account and thus offers an excellent base to make design selection of solar cells.

3.3.1 Sample cell structure

A typical configuration can be an heterojunction solar cell with full metallic back contact, as shown in Figure 3.1. This structure allows to efficiently separate the electron and hole pairs generated by light excitation due to the photovoltaic effect.

Another significant property of the solar cell is the texturing of the oxide layer employed for passivation, in the case of Figure 3.1 the ITO, turning this layer into an anti-reflective coating (ARC), which enhances the absorption and trapping of light. This is achieved by applying a layer of dielectric material with a certain thickness and refractive index which favours the transmission of light and reduces the reflection at certain wavelength

when placed between two materials, in this case the Silicon wafer and air [55]. When this ARC is textured, any possible reflection is also reduced by enhancing the possibilities for the light to bounce back into the cell [56]. On the other hand, the ARC can also passivate the Silicon surface in order to reduce surface recombination and therefore loss of current.

Regarding bifacial cells, it is to be notede that the GP4 can only have one light source. However, if the structure of a cell is reversed, the behaviour of the cell when irradiated from the rear side can be predicted. Therefore, it is simple to adapt the software to bifacial use, however double the computational time has to be spent.

3.3.2 Number of rays

Ideally, infinite number of rays would be simulated in order to obtain the optimum results. However, the large the amount of rays, the more time consuming it will be and therefore the usability of the toolbox drops. For this reason, it is important to find the right balance between amount of rays and accuracy of the results.

Figure 3.6 shows the absorption of the cell described in the previous subsection, plus EVA and glass layer, for light coming randomly from all angles and 600 nm wavelength. This figure also shows the absorption of the inner c-Si layer of the cell, and the error bars corresponding to the standard deviation from a dataset of 10 runs. It is observable that when the absorption is only dependent on a flat surface, such the total absorption of the cell, since the glass is flat, less amount of rays are required in order to achieve the same accuracy as it is needed for absorption values that rely on textured surfaces, such as the c-Si layer absorption, since the light passes through the inverted pyramid texture. This is understandable since such a texture allows the light to bounce in more directions and thus a significantly large number of rays will provide more accurate absorption estimates. It is also interesting to observe how for the 1000 rays simulations the results are more spread than for 100 rays, which is not expected. This is an artifact caused by a non entirely random angular distribution of incident light on the GenPro4 software, as discussed with the creator of the software.

Overall, it is concluded that 100 rays is the optimum trade-off in terms of computational time and accuracy of the results since it is able to give cell absorption values accurate to the $\pm$ 0.8% and c-Si absorption values accurate to the $\pm$ 0.4%.

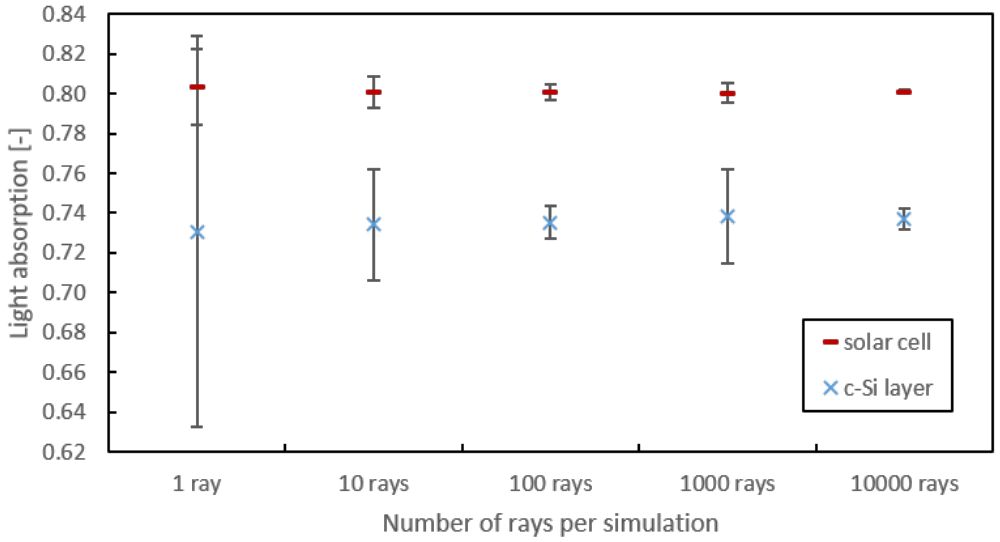

FIGURE 3.6: Simulated light absorption as a function of simulation ray number for a heterojunction solar cell including EVA and glass layer. Error bars represent standard deviation.

3.3.3 Wavelength bins

As stated in the scope of this thesis, one of the goals of this work is to be accurate when considering optical absorption of light with different spectrum. This difference in spectrum can be caused by atmospheric conditions, such as the difference in Air Mass that the light has to go through at different times of the day, and also caused by different reflective ground level surfaces, which can reflect the light in several spectrums. Therefore it is important to understand wavelength dependent absorption of the solar cell, including the EVA and glass layers, its reflection, transmission and the absorption corresponding to the c-Si layer, which will generate the current.

To analyse down to which spectral resolution it is necessary to go to obtain accurate results, the following work is performed. The spectrum is divided in 100 nm wavelength bins, following the guidelines of the international norm for solar simulator light quality assessment IEC 60904-9 [57]. Since this bin distribution is employed when performing experimental power measurements of PV modules, it is considered suitable also for simulation predictions. Each bin absorption value, however, can be calculated from averaging the aborption values of smaller wavelenght bins. In order to assess this, the absorption for each bin is calculated at different spectral resolutions. This means that, for example, for a resolution of 100 nm, the absorption value of the bin between 300 and 400 nm is calculated by running a simulation at 300 nm, one at 400 nm, and averaging the values. Similarly, for a resolution of 50 nm, the average of 300, 350 and

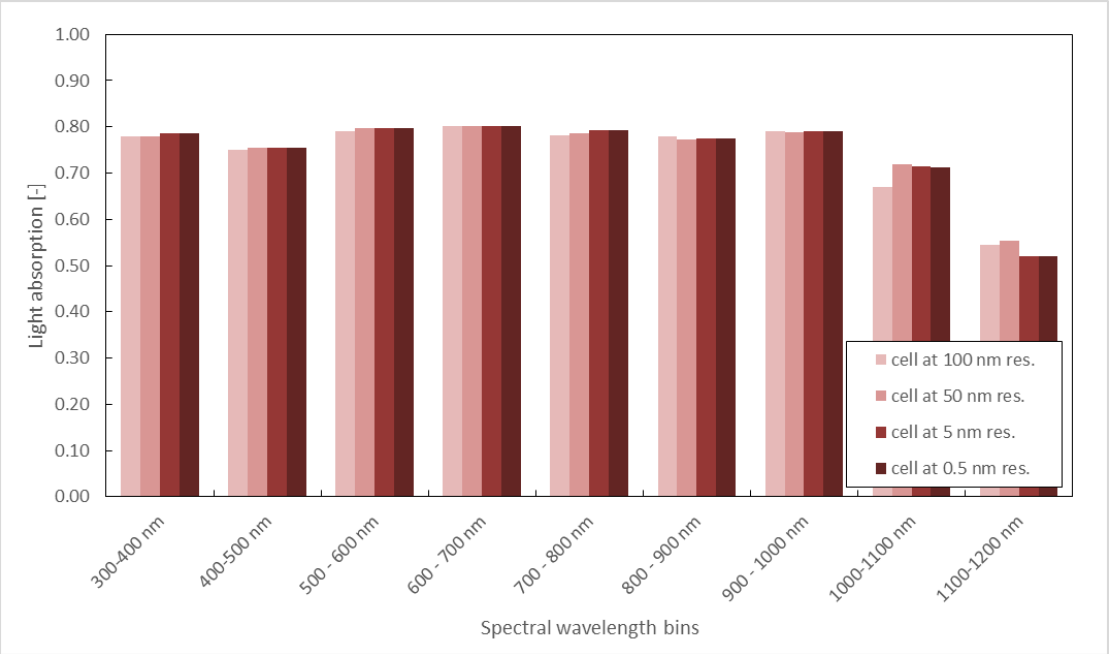

FIGURE 3.7: Simulated total light absorption as a function of wavelength for a heterojunction solar cell including EVA and glass layer. Colours represent different simulation spectral resolution.

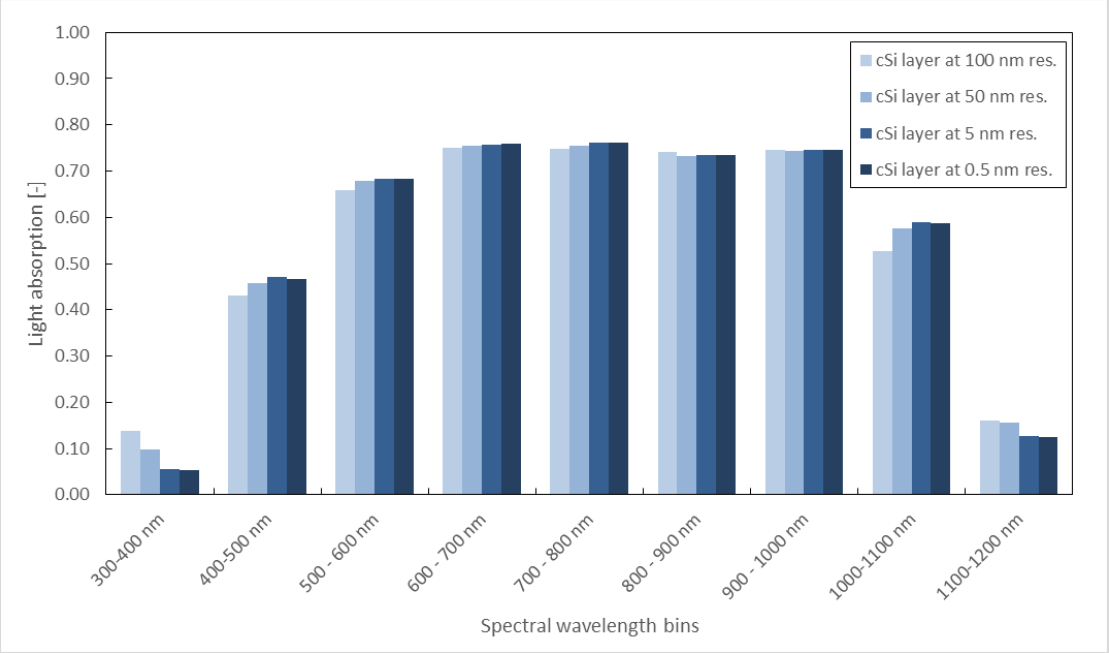

FIGURE 3.8: Simulated c-Si layer absorption as a function of wavelength for a heterojunction solar cell including EVA and glass layer. Colours represent different simulation spectral resolution.

400 nm simualtions runs is taken. Runs are performed with 100 rays, as concluded in the previous subsection, coming from all angles. Figure 3.7 shows the light absorption of an entire heterojunction cell, including the EVA and glass layers for both sides. It is seen that absorption does not vary more than 0.2 % for spectral resolutions between 5 nm and 0.5 nm, therefore absorption value is assumed to remain constant from 0.5 nm onward. It has to be noted that the international norms that define AM 1.5 spectrum such as IEC 60904-3 [58] use a resolution of 1 nm for the range between 300 and 1200 nm, therefore the simulated absorption value with a resolution of 0.5 nm is taken as 'true' value. For a resolution of 100 nm and 50 nm absorption value can suffer relevant deviation from the true value down to -4.1 % and up to 3.5 %, respectively. This information has to be accounted for when performing the complete bifacial toolbox simulation in order to calculate the simulation error. Ideally it should be possible for the user to choose the degree of accuracy depending on the time that is willing to spend on the simulation, and what are his/her requirements.

Similarly, Figure 3.8 shows the light absorption of the cSi layer within the previous cell. This value is directly proportional to the current generated by the cell and therefore it is highly relevant to accurately determine it. It is seen that resolutions of 100, and 50 nm deviate as much as 8.5 and 4.4 % from the 'true' value in some bins, specially close in the UV area, while 5 nm remains always within 0.5 % deviation maximum.

In conclusion, using 100 nm resolutive simulations can overestimate the absorption of light in the ultra violet area, although it provides a good match in the visible part of the spectrum. Therefore not large differences are expected in energy yield compared to more detailed spectral simulations such as 50, 5 and 0.5 nm.

3.3.4 Angle of incidence bins

As it occurs with the wavelength, the absorption of cell and cSi layer and the transmission and reflection also depend on the angle of incidence. When most of the light is direct, using the correct absorption values for that specific light angle of incidence is specially important, since absorbance decreases dramatically at low angle of incidence. When light is diffuse, meaning that it comes evenly from all directions, the average absorption value among all angle of incidence shall be employed. Therefore, it is important two elements in this subsections. First, accurate absorption value per angle and secondly accurate average absorption value. Again, computational time is important and thus different levels of angular resolution are assessed when predicting these values.

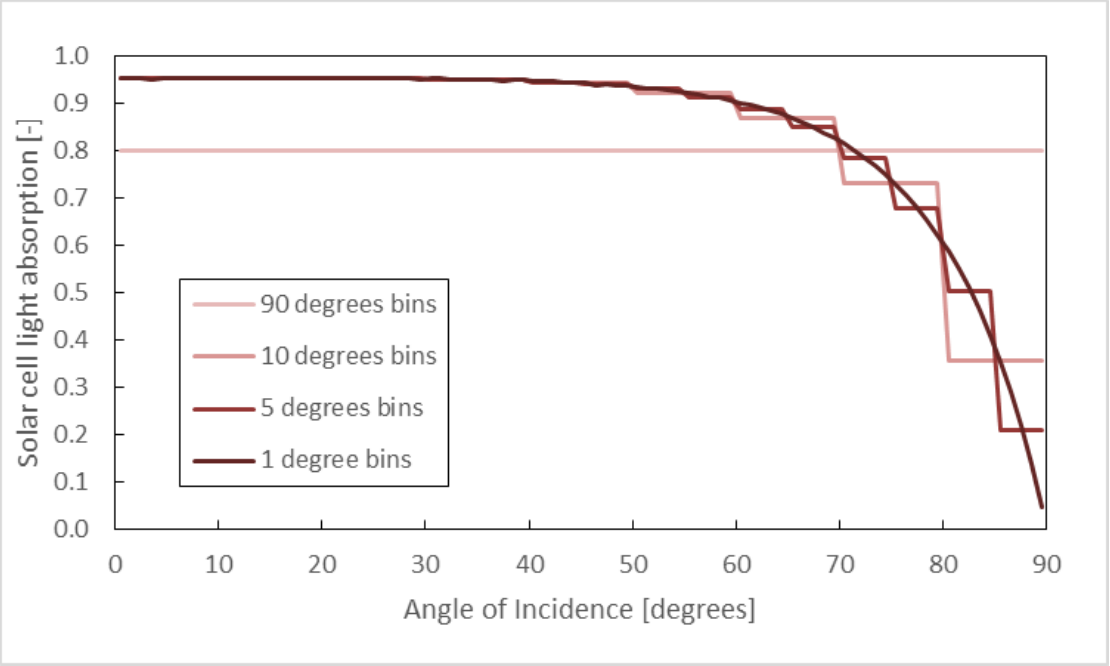

FIGURE 3.9: Simulated total light absorption as a function of angle of incidence for a heterojunction solar cell including EVA and glass layer. Colours represent different amount of angular bins.

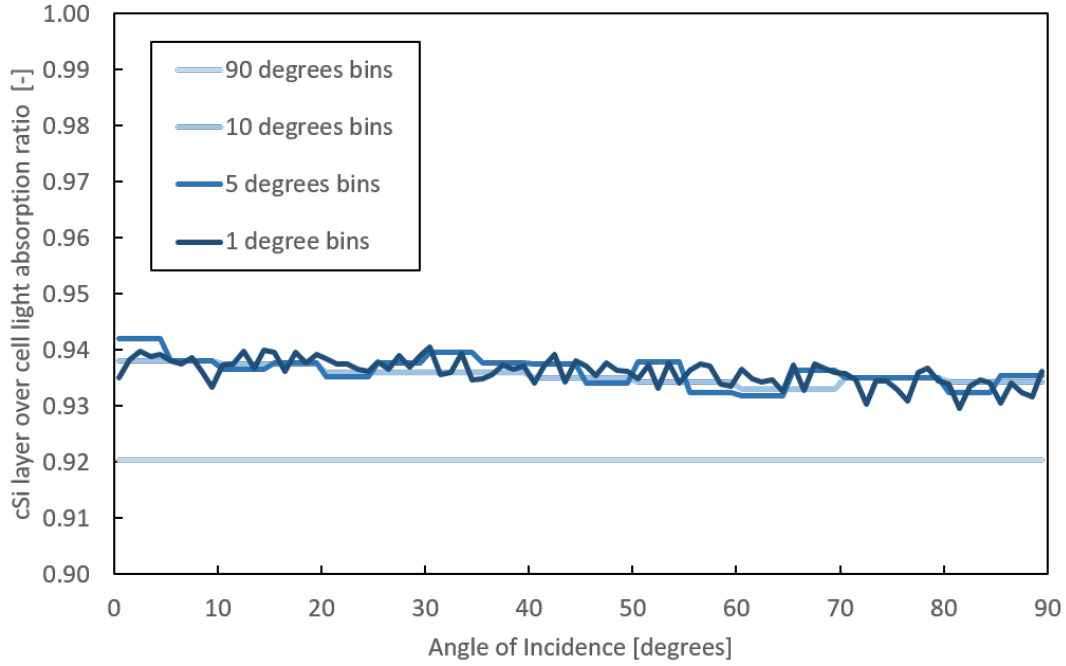

FIGURE 3.10: Simulated c-Si layer absorption over total light absorption as a function of angle of incidence for a heterojunction solar cell including EVA and glass layer. Colours represent different amount of angular bins.

No international standard has been yet published on angle of incidence measurement of photovoltaic devices therefore one degree resolution is arbitrarily taken in this case as 'true' value, and 5, 10 and 90 degrees resolution steps are compared. Figure 3.9 shows the absorption of the previously presented heterojunction cell with EVA and glass layer as a function of angel for the aforementioned angular resolution bins. It is seen that while at small incidence angles between 0 and 40 degrees only the 90 degrees bin simulation induce a relevant error, of down to -15.3 %, while the 10 and 5 degrees bin show a maximum disagreement of 0.2 and -0.2 %, respectively, when compared to the true value. For greater angle of incidence, these disagreement grows to 75.2, 30.9 and 16.1 % for 10, 5 and 1 degree angular bins, respectively. Regarding the average absorption value at all angles, which as said is relevant for diffuse light absorption, it differs -4.8, 0.0 and 0.0 % for 90, 10 and 5 degree angular bins when compared to the 1 degree angular bin value.

Regarding the absorption of the c-Si layer, Figure 3.10 very interestingly shows the ratio between it and the total cell absorption, including EVA and glass layers, and shows that for all the resolution bins, the ratio does not vary more than 3.0 %. Regarding the average value, which is useful for diffuse light situations, the differences versus the 'true' value are of -1.6, 0.1 and 0.0 % for the 90, 10 and 5 degrees angular bin resolutions.

Overall, it is observed that a single angular bin with 90 degrees range from where all the light rays randomly come does not only underestimate and overestimate absorption at small and large angles, but yields an inaccurate average absorption value, relevant for diffuse light. Regarding other angular bin options, 10 degrees is found to be accurate enough in terms of average absorption values and at small angle of incidence for direct light. Although it differs at large angle of incidence, its effect on the annual energy yield will rely on how often the situation of direct light at large angle of incidence might occur.

3.3.5 Assumptions of the model

After light absorption, and once the electrons and holes, also known as carriers, have been separated, they have to be collected at both ends of the cell, in order to create an electric circuit. To do so, metallic contacts are employed. On the front side, where the light is coming from, these contacts have to be of reduced area in order to avoid shading, thus they are implemented in form of busbars.

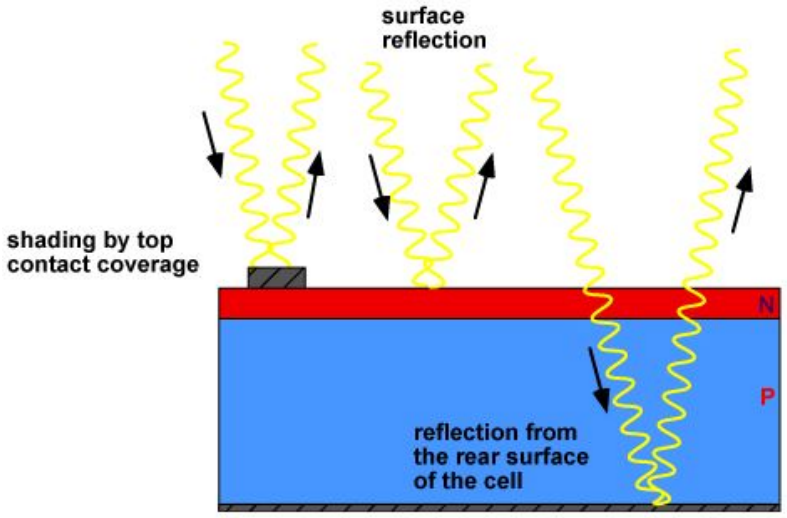

FIGURE 3.11: Graphic explanation of the reflective losses that might happen to a PV cell, taken from http://www.pveducation.org/pvcdrom/optical-losses

Figure 3.11 shows an schematic of the different reflection losses that might occur in a solar cell. While the reflection of the different layers that form the cell is taken into account by GenPro4, it is not the case for the shading caused due to metallization. Besides shading, metallization has as well an effect in terms of internal reflection.

The simulations performed with this model do not consider optical losses due to metallization and therefore their effect must be accounted a posteriori with a correction factor, if needed. This correction factor, however, is not included in the scope of this thesis.

3.4 Application to case analysis

After understanding the effect of each simulation parameter such as number of rays, wavelength simulation bins and angle of incidence bins on the accuracy of the simulation output, a real case analysis is performed in order to validate the cell optical block. In line with the INNOZWA project, the cell level alternatives to be discussed are either monofacial or bifacial technology.

3.4.1 Monofacial vs bifacial

To do so, a comparison between current generation of similar heterojunction solar cells with monofacial and bifacial functionality when light is only incident from the front at AM 1.5 spectrum conditions is carried out. It is expected that the monofacial cell generates more current since the rear metallization plate can reflect light back into the cell, whereas for the bifacial cell this light will be transmitted.

The cell structure is the same, consisting of an n-type wafer with i and p layers on the front and i and n layer on the rear, in order to create the hetorjunction. ITO is applied to the front and they both have glass and EVA layers on front and rear side, however the monofacial cell has a rear silver plate that acts as carrier collector, while the bifacial cell has another ITO layer, similar to the one in the front, in a highly symmetric structure.

The simulations are carried out, as discussed in the previous sections, with runs of 100 rays every 100 nm and with the rays coming randomly within angular bins of 10 degrees. The absorption, reflection and transmittance results are averaged over all angular bins and presented in Figure 3.12 and 3.13. Finally, these results are weighed with the corresponding photon content of the spectrum AM 1.5 and translated into actual current density. The difference begtween current density between the bifacial and the monofacial cell is presented in Figure 3.14. As it can be seen, for the left part of the spectrum both cells behave in the same manner, however, as the spectrum approximates to the near infrared, the transmittance of the bifacial cell increases and as consequence its c-Si layer absorption and reflection decreases. This is as expected, since the bifacial cell does not have a metallization plate that can reflect light back in the cell. As an overall consequence, the current generated by the bifacial cell is 0.4 mA/cm^2 less than the monofacial cell, which translates into 1.3 %. This is in agreement with current literature values [59]. Note however that this loss in generated current is obviously compensated by the fact that bifacial cells and modules can efficiently convert the light incident on the rear side to electricity.

Regarding the rear side performance, the bifacial cell structure employed in the simulation can be flipped and therefore the rear side performance can be analyzed. Due to the high symmetry of the cell, and to assuming no metallization, the performance results are extremely similar to those of the front side, and therefore not included in this section.

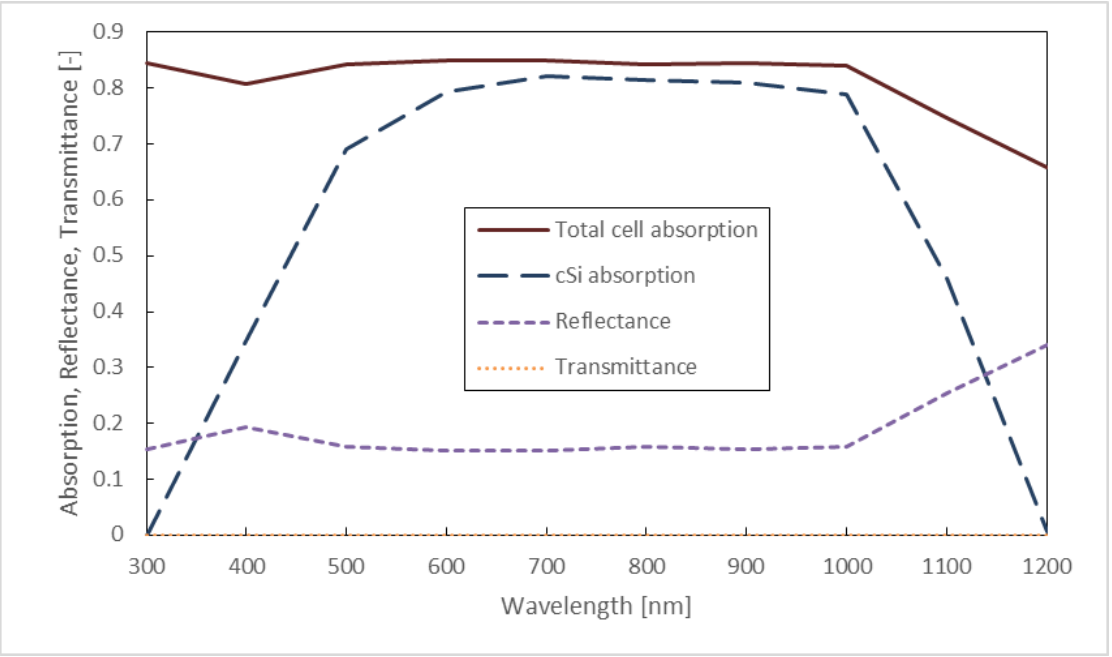

FIGURE 3.12: Simulated cell and cSi layer absorption, reflection and transmission for a full monofacial heterojunction solar cell, including EVA and glass layers, as a function of wavelength.

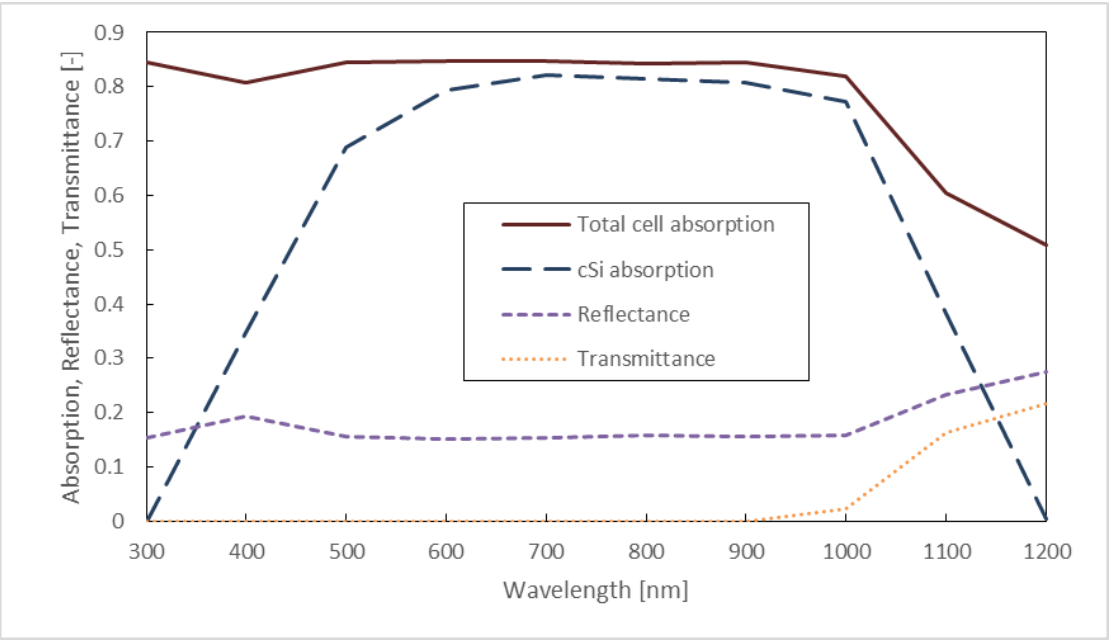

FIGURE 3.13: Simulated cell and cSi layer absorption, reflection and transmission for a full bifacial heterojunction solar cell, including EVA and glass layers, as a function of wavelength.

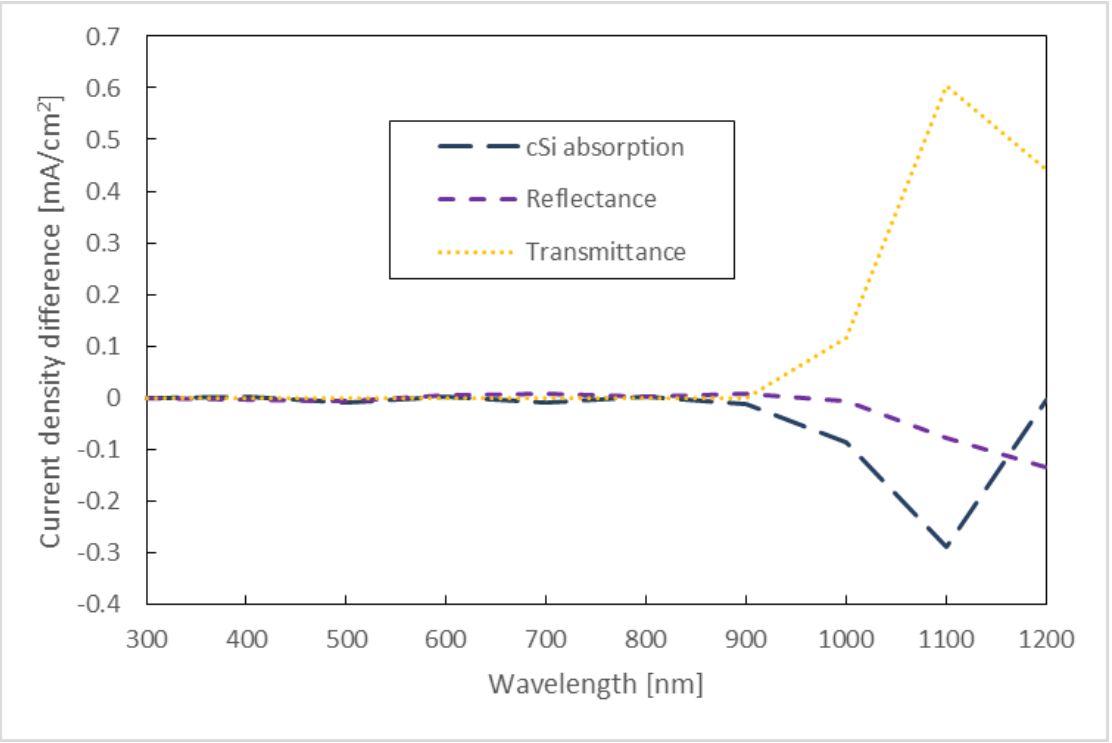

FIGURE 3.14: Difference in current absorbed by cSi layer, transmitted and reflected between a bifacial and a monofacial heterojunction cell under AM 1.5 spectrum.

3.5 Conclusions

The first block of the simulation toolbox has been presented in this chapter, together with three algorithms to extract the desired output, which consists of absorption of cell and c-Si layer, reflectance and transmittance of the cell, as well as other electrical parameters that can be retrieved from datasheets or literature.

The focus has been put in assessing the accuracy of the absorption, reflectance and transmittance values, since it allows to greatly customize and evaluate the cell structure in terms of current generation. Three simulation parameters have been pointed as key to determine this accuracy: number of rays per simulation, wavelength and angle of incidence simulation bins.

The most suiting simulation parameters for cell level (including EVA and glass layers) optical simulation that balance accurate results and reasonable computational time have been discussed. These have been found to be 100 rays per run, simulations every 100 nm wavelenght and a set of 9 simulations per wavelength at different angle of incidence.

Finally an electrical current generation, reflectance and transmission comparison between almost identical heterojunction solar cells with monofacial and bifacial functionality has been analyzed and the results matching expected literature values. Therefore it is concluded that the Cell Technology Block output under the investigated simulation parameters is suitable as input for the rest of the toolbox.

Chapter 4

System Setup Block

Secondly, the system design goal is to understand how sensitive will be a module installed in a certain setup. This includes tilt, azimuth, mounting beams, horizon that shades the module and albedo of the ground. Therefore the input must be all the details of the 3D composition and the absorption, reflection and transmission of the surfaces involved. In this chapter, the PV system construction of the site is built and the influence on the irradiance received by the cells analyzed. For such purpose, a code to build 3D setups using the LUX and Matlab environment shall be developed.

4.1 Concept, input and output

Real field PV installations usually differ from the ideal situation shade free optimum tilt and azimuth situations. Therefore for making accurate energy yield predictions it is key considering the influence of the PV module design and the surroundings into the irradiance received by the cells and its proportional current generation.

With this goal in mind, it is the purpose of this chapter to develop the next block of the toolbox, which it is referred as System Design block. The input for this block is the geometry of the PV module and its surroundings, including far horizon shading, and the optical properties of the different elements, such as the PV module, the mounting, the ground, etc. in terms of absorption, reflection and transmission, as function of wavelength and spectrum. Similarly as done in the Cell Technology Block, the dependence on wavelength and angle of incidence will allow to carry out more accurate energy yield predictions that will adjust to different locations of the world. It will also become very

useful for taking into account spectral changes in the albedo because, as reported in literature, different surfaces project albedo with different spectrum, which will make the electricity generation of the rear side of a bifacial PV module vary significantly. The output therefore shall be a matrix containing the cell light absorption for that very technology and system design as a function of the altitude and azimuth of the incoming light.

4.2 Possible approaches and algorithms

The algorithm of the system design block is explained in this section. Two methods are presented, the 'Build your own System', which is based in the detailed modelling concept described above, and the basic tilted setup, which aims to offer a simple alternative for fast preliminary energy yield assessments.

4.2.1 Build your own system

This approach aims to mimic the real outdoor situation into a sandbox and afterwards perform ray tracing of light incident from all possible angles in order to understand how much light of the incident ends up being absorbed by the cell. This is the definition of sensitivity. The output aim is therefore to establishing a matrix of the sensitivity of the cells depending on azimuth an altitude, for front and rear side, in case of a bifacial module, and per every wavelength. The algorithm of this method is presented graphically in Figure 4.1.

The input necessary to generate the sandbox environment and the posterior sensitivity map is defined in three categories: geometrical, optical and sensitivity map input. For the geometrical category, firstly the number of cells has to the considered, then the module dimensions, such as thickness and intercell spacing. Other parameters are the tilt and height of the module, the mounting structure, the distance between modules and the reflectors, if any, placed around the module. Once this input has been introduced, a expressly developed Matlab code, called 'SetupBuilder', which is explained in the following section, runs and builds the sandbox.

The optical input aims to define the absorption, reflection and transmission of the different elements involved in this sandbox, as a function of wavelength and angle of incidence, if possible. Of course, the A,R,T of the cell, including the glass and EVA layers, is the

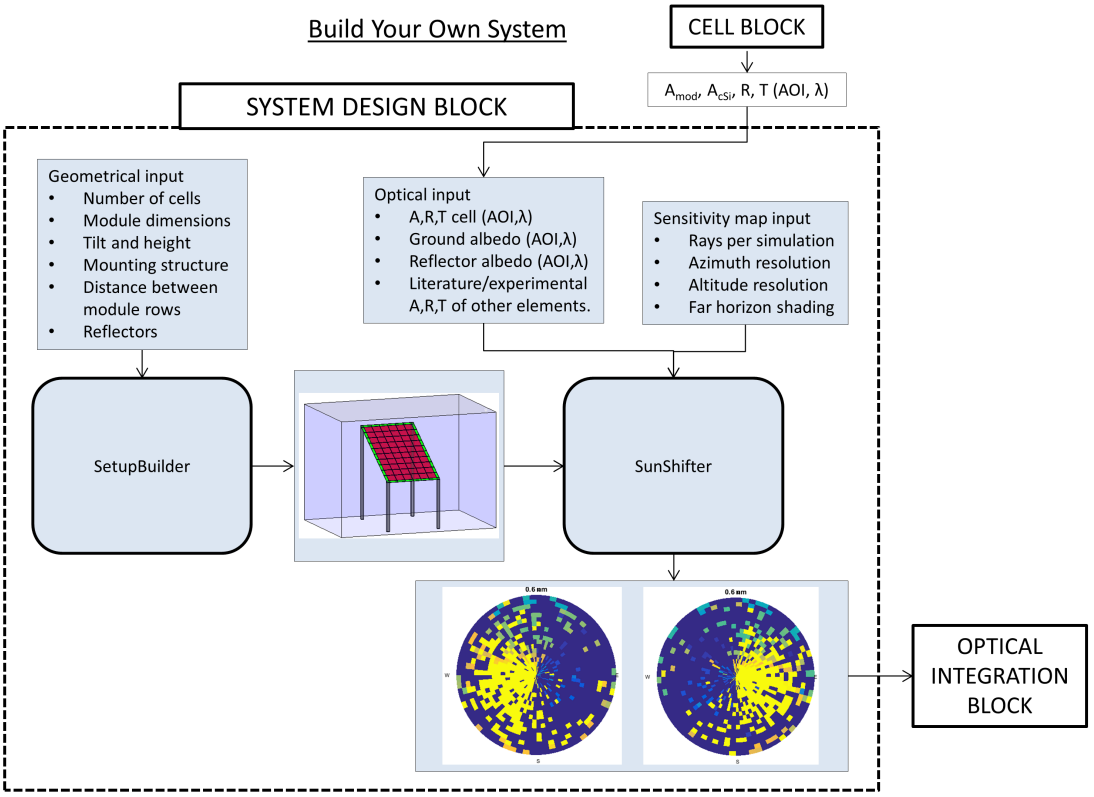

FIGURE 4.1: Algorithm for applying the Build your own design approach.

output of the Cell Technology Block. For the rest of surfaces, literature or experimentally measured values can be employed. With this information, the LUX ray tracer can be started and an assessment of light absorption for that incident angle of incoming light is reported, thus calculating the sensitivity of the cell to that azimuth and altitude.

Light in real outdoor conditions, however, does not come only from a single spatial point but from several, specially in the diffuse light case. Therefore, a matrix of sensitivity points must be generated. For this step some input is needed, regarding the resolution of the matrix and the amount of rays used per simulation. Finally, for a more accurate prediction, input on the far horizon shading needs to be applied, since it will obviously affect the sensitivity of light coming from that direction. This can be done for instance employing the Horicatcher technique.

4.2.2 Basic tilted setup

Finally, an alternative for simplistic calculations is also provided, for this situation, only the tilt and azimuth of the PV module, as well as the albedo of the ground is required

as input. This approach, however, is not added to this first version of the toolbox since it falls out of the scope of this thesis.

4.3 Constructing the 3D setup

This section describes the manner in which the 'SetupBuilder' Matlab code is developed and the steps in which builds the sandbox. It is to be noted that the ray tracer software that will be used afterwards is the 'LUX' Matlab based software developed. For this reason, the 'SetupBuilder' works also with vertex and facets defined by spatial coordinates.

4.3.1 Geometry of the module

As starting point, it is necessary to note that the optical Cell Technology Block already considers the EVA and glass layers, therefore these can be ommitted in the system design block. This has the advantage of saving computational time by not having to generate those layers and consider their absorption every time that a new sensitivity data point is calculated. On top of that, the ratio between cell absorption and c-Si layer absorption remains constant through different angle of incidences, as shown previously in Figure 3.10. Therefore the sensitivity map can just be corrected by this factor for any azimuth and altitude.

Taking that into consideration, the module building can start. It is required by the user to fill in information on cells per column and cell per row within the module. Therefore the module design can consider mini modules of 1 or 4 cells and commercial modules such as 60 or 72 cells. Of course other amounts are also possible. Afterwards, the module thickness, the intercell spacing and the edge spacing is also requested. With these parameters, the 'SetupBuilder' finds out the right coordinates of the vertex of the module and of every cell, and unites them into facets. Figure 4.2 shows the corner of a simulated cell and module produced using the 'SetupBuilder' code.

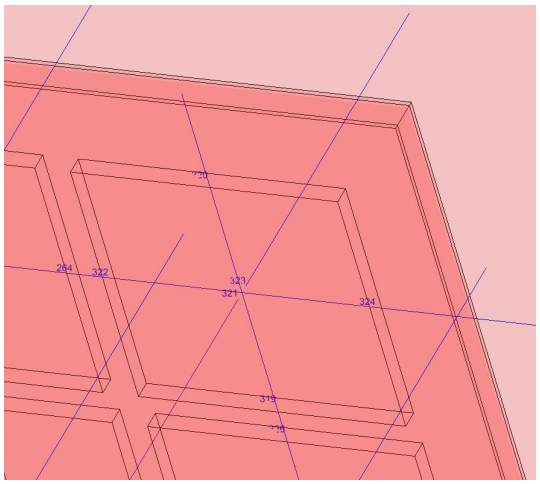

FIGURE 4.2: Example of a cell within a module generated using the 'Setup-Builder' code to which 'LUX' ray-tracing is performed later.

4.3.2 Tilt, height and orientation

As it is well known, the surface orientation of the PV module, defined by its tilt angle and the azimuth that is facing, plays a big role in he amount of light absorbed by the cells. So does the height at which the PV module is installed, due to being more or less sensitive to the reflected light, as well as a difference in the manner that shading by surrounding elements affects the PV module.

It is to be noted, however, that the output of the system design block is a sensitivity map which can be rotated around azimuth due to its hemispherical composition. Therefore it is not necessary to generate different sensitivity maps for modules placed with different azimuth because the output will be the same but rotated over the central point. Therefore, from the three parameters presented in this subsection, the only two that will have an impact on the sensitivity map output are the tilt angle and the height to the ground.

Therefore the 'SetupBuilder' program is improved by adding code that is able to rotate the module coordinates following the user input, and move them in the z direction adjusting to the desired height.

4.3.3 Mounting and reflectors

At this point of the sandbox, there is a tilted PV module floating at a certain height over the ground. In real life, however, PV modules do not levitate but are subjected by

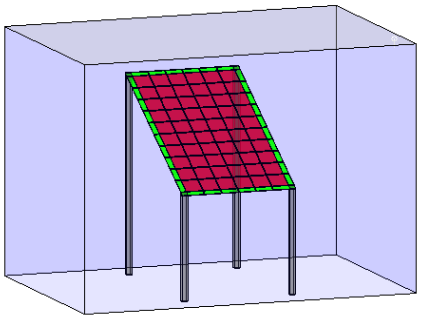

FIGURE 4.3: Example of a PV module with four legged mounting structure generated using the 'SetupBuilder' code to which 'LUX' ray-tracing is performed later.

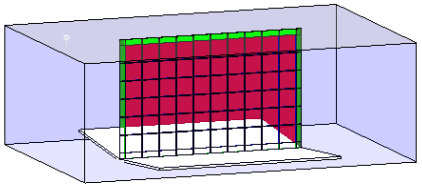

FIGURE 4.4: Example of a vertical bifacial PV module with reflectors generated using the 'SetupBuilder' code to which 'LUX' ray-tracing is performed later.

some sort of mounting structure. This mounting structure has also an optical impact on reflected light by causing shading, which is specially relevant for tilted or horizontal bifacial PV modules in which the rear side is receiving mostly ground reflected light. While many different mounting structures for PV modules exist, in this thesis a regular four legged structure is implemented, as shown in Figure 4.3 leaving room for future additions.

Besides the mounting structure, another surrounding structure that is of interest of researchers, although not that often implemented in real life, are light reflectors. The reflectors can make direct light that would have not been collected by the panel bounce into its surface, thus enhancing the electrical generation. This is specially interesting for bifacial PV modules placed vertically, since the reflectors can be placed flat around the module, not causing any shading and reflecting plenty of light, some falling into the module. Thus, reflectors are also implemented in the 'BuilderSetup'. This is done by creating flat panels starting from the bottom edge of the PV module and tilting them

at the desired angles, similarly to how it is done for the PV module. An example setup with reflectors generated with the program is shown in Figure 4.4.

4.3.4 Distance between panels

The last geometrical input in the scope of this 3D structure considered by this work is the distance between panels in case there is more than one. The 'LUX' ray tracing software has the feature of teleporting the light rays from one surface to another, if desired. Thus, each sandbox unit can be considered as an infinite array of sandbox units if teleportation is performed between the external walls. For example, if a ray falls into the right wall is the being teleported into the left wall and goes inside the sandbox again. Therefore, if the sandbox width is the same as the panel width it effectively means that one panel is immediately next to another one. Similarly occurs for the sandbox length in front of the panel, which will translate with the distance between rows of panels. Therefore a single standing panel shall be placed in a 'big' sandbox, in such a way that the shading due to nearby panels has negligible effect. For simulating a PV farm rows of modules next to each other and at a certain distance from the row in front, a sandbox of the same width of the PV module and with a certain lenght equivalent to teh distance between rows shall be applied. More details on the functionality of the teleporting property is presented in the next subsection.

4.4 Optical properties of the surfaces

The geometrical construction of the sandbox has been presented in the previous subsection. The present step is to assign absorption, reflection and transmission properties to the different surfaces as a function of angle of incidence and wavelength. 'LUX' software contains an existing library of optical properties for different standard materials, such as glass, aluminium, and air, among others. It is to be noted that for the cell, properties come as an output from the cell architecture block.

4.4.1 Module absorption, reflection and transmission

The PV module built in the sandbox consists of different rectangular prisms which can be distinguished in two groups: the cells and the ones forming the intercell spacing. For ray

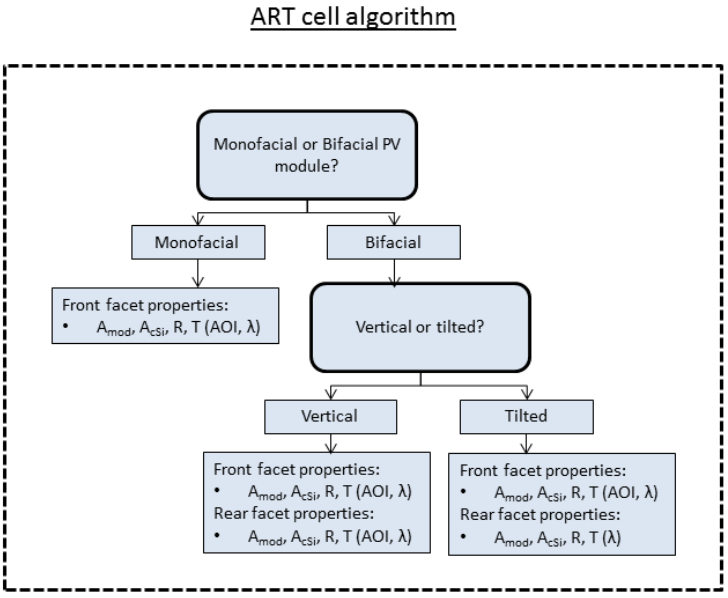

FIGURE 4.5: Algorithm for selecting the optical properties input for front and rear surface of every cell unit built with 'SetupBuilder' and ray-traced using 'LUX'.

tracing purposes, it is necessary to assign each polyhedron a certain absorption, reflection and transmission behaviour at each wavelenght and/or define the two materials at each side of every facet, whose properties are retrieved from the library. The properties of the front side output of the Cell Technology Block, as a function of wavelenght, are assigned to the front facet of each cell. Regarding angular dependence, the value to apply is depending on the azimuth and altitude of the incoming light, as well as with the ratio of diffuse light. Similarly, the rear side is assigned with the rear side cell properties output from the cell architecture block, as a function of wavelenght. For the rear side, however, the angular dependence is managed by using the average angular absorption, reflection and transmission values, since it is estimated that the rear side will rely mostly on diffuse light. The exception case, however, is when the bifacial panel is placed in vertical position, in which the rear side properties are managed in the same manner as the front side properties, explained above. Regarding the edge absorption, is quite negligible considering the small surface compared to the front and rear, and thus standard c-Si properties form the library are applied to it. Figure 4.5 shows the algorithm employed for assigning optical properties to the cell, as explained in this paragraph.

Regarding intercell elements, the EVA component is neglected and it is assumed that they are made completely of glass, thus assigning standard glass optical properties form the LUX library.

4.4.2 Ground, reflectors and mounting structure albedo

The mounting structure is assumed of being made of aluminium and its optical properties taken form the library. This is because the mounting structure will have a bigger impact on the light absorption of the PV module in terms of shading, but not of reflected light, thus the reflected light spectral distribution of the mounting beams is not important as long as the transmitted light for the 300 to 1200 nm range is zero, which is the case of the library values.

Regarding ground and reflectors albedo, a single values for all wavelenghts and angle of incidence can be input, as it is traditionally reported in literature. However, if experimental values obtained with an spectrometer are feasible to retrieve, optical properties of their surfaces can be input as a function of wavelength. For angular dependance, it is assumed in this thesis that ground and reflectors behave in the same manner for all angles of incidence light, and scatter it perfectly over all directions.

4.4.3 From single module to PV farm

The remaining sandbox surface to be assigned properties are the walls, since the ceiling is the ray emmiter surface. As explained in the previous section, the walls can teleport light rays incident into them to the opposite wall, which emmits them back into the sandbox. Therefore, its is assumed that for all wavelengths and angle of incidence the walls are a perfect transmitting surface, with no absorption or reflection. Again this is useful for simulating optical effects of PV modules placed into arrays like in a PV farm. Single standing modules can be simulated by making the walls of the sandbox relatively large compared to the size of the module.

4.5 Ray tracing and SunShifter

The geometrical setup and the optical properties have been assigned to the different elements. Therefore, it is already possible to run ray-tracing simulations on the sandbox with light coming from the ceiling at different angles and azimuths. For this purpose, the 'SunShifter' program is coded giving instructions to the 'LUX' ray tracing software and managing its ouput converting it into sensitivity values for every desired wavelength. Later, every single sensitivity values is put into a Sensitivity Map, having one per every wavelength step. An assessment on how many rays are necessary per simulation in order to produce an accurate prediction is also assessed in this section.

4.5.1 Output management and sensitivity

When a ray tracing simulation is performed, a number of rays from a specific wavelength are emmited from the ceiling at a certain direction, corresponding to the desired altitude and azimuth. Then these rays interact with the different surfaces whithin the sandbox, and can be aborbed, reflected and transmitted. Finally, the relative absorption of the different elements, such as the PV cells, the intercell spacing and the ground, among others, is reported by the 'LUX' ray tracing software as a unitless values over one. It has to be noted that the bigger the sandbox is compared to the PV module within it, the lower the absorption value of the PV cells. This also holds true for flat panels were shading between panels is negligible, thus proving that it is a pure matter of relative surface between the PV panel and the light emmitting source surface.

In real field conditions, however, the size of the area of the PV module surface is negligible respect to the area from which light is coming from. Therefore, it is important to make the aborption output of the 'LUX' ray tracing software independent of the area of the sandbox. To do so, the definition of Sensitivity by Muthukumar [32] is adapted as shown in Equation (4.1), where $A_{PV\,cells}$ is the total front surface area of PV cells inside the sandbox. Therefore a Sensitivity value per altitude and azimuth of the incoming light and per wavelength for the PV module is reported. It is to be noted also that the sensitivity value can be greater than one if, for instance, reflectors are employed. Finally, it is to be noted that for bifacial modules the ray-tracing software can distinguish between front and rear surface, thus providing two sensitivity values.

$$Sensitivity = \frac{Light \quad intensity \quad on \quad a \quad surface}{Light \quad intensity \quad of \quad the \quad source} \tag{4.1}$$

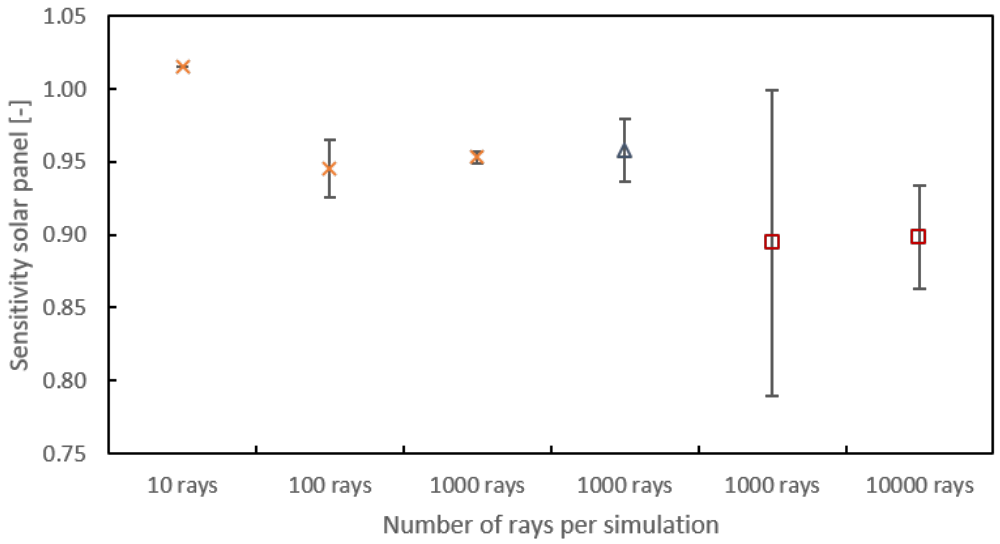

FIGURE 4.6: Sensitivity output of a flat monofacial solar panel within a sandbox, as a function of number of rays. Symbols represent the sandbox size, being crosses 0.8 per 1.4 m, triangle 2 per 3 m and squares 8 per 12 m.

4.5.2 Number of rays

Now that the output of the block is defined, it is to be analyzed its accuracy. The accuracy of the output is mostly going to be dependent, as it was the case of the Cell Technology Block, on the number of rays used in the simulation. The size of the sandbox compared to the size of the PV module, however, also plays a role, as mentioned in the previous subsection, since less rays will interact with the PV module surface.It has to be remembered that the sandbox size is not an arbitrary value but is related to the distance between panels in a row. Therefore the guidelines on the relation between sandbox size, number of rays and accuracy need to be considered to assess the accuracy depending on the simulated system setup.

With these considerations in mind, an analisys on the effect of number of rays and relative box size on the sensitivity value output is carried out in this subsection. Figure 4.6 shows the sensitivity output of a flat monofacial solar panel of 1 per 1.7 m to perpendicular light at 600 nm, as a function of number of rays. Symbols represent the sandbox size, being crosses 0.8 per 1.4 m, triangle 2 per 3 m and squares 8 per 12 m. Error bars represent the standard deviation out of 10 runs. The output of the Cell Technology Block, which is used in this simulations as input, predicts that the absorption value of the PV cell to perpendicular light at 600 nm wavelength is of 0.95. Therefore for the situation presented in Figure 4.6 it is expected a sensitivity value close to that. For sandbox size smaller than the PV module itself, 100 rays are enough to

get close to the absolute value with a small error of ± 0.02. It is to be noted, however, that a smaller number of rays such as 10 repeat always the same output, therefore the standard deviation is zero. This is due an artifact with the LUX ray tracing in which for low number of rays all the rays depart form the same point on independent simulations. The output for 10 rays overestimates sensitivity by 0.06 absolute value. For a box size of 2 per 3 m, which represents approximately 3 times the area of the PV module, the average sensitivity value out of 10 runs matches the expected one and the small sandbox one, however for the same number of rays, 1000, the standard deviation grows from 0.00 to 0.02 absolute value. For relatively big sandbox of 8 per 12 m, with a surface approximately 50 times greater than the PV module, the standard deviation with 1000 rays grows to 0.10, being necessary 10000 rays to reduce it to 0.04. It has to be noted also that the absolute sensitivity value for such case decreases to 0.90. This difference in absolute value is believed to be due to the small number of runs, 10, which is not enough in the big sandbox case to assess accuratelly the correct mean value. It ha to be noted, however, that every 10000 rays simulation takes 13 seconds to process, therefore it is considered that the trade off between accuracy and computational time is already enough at this level.

4.5.3 The SunShifter

During daytime, light coming in a direct manner from the Sun or reflected diffracted by other elements in a diffuse way can arrive form any direction from the hemisphere above the ground. Therefore, there azimuth range goes for 360 degrees, making a full circle, and the altitude range of incident light can vary from 0 to 90 degrees, considering 90 degrees as when the light is coming from exactly the center of the hemisphere. Therefore ideally it would be interesting to know the sensitivity of the PV module per every point of the hemisphere from which it is incident, with the highest resolution possible. The 'SunShifter' program is developed expressly to run this operation, meaning to run the 'LUX' ray tracing software for all desired altitude and azimuth and for the selected wavelength bins, while assuring that the correct absorption, reflection and transmission values of a cell for the given wavelength and angle of incidence are employed as input. The guidelines on the optical properties to assign at different altitude and azimuth are explained in Figure 4.5. 'SunShifter' is also responsible of assigning the right albedo values as a function of wavelength for the ground and reflectors surfaces.

The altitude and azimuth resolution level is left to the choice of the user in this toolbox. However, an assessment on the accuracy in the results depending on it is carried out in

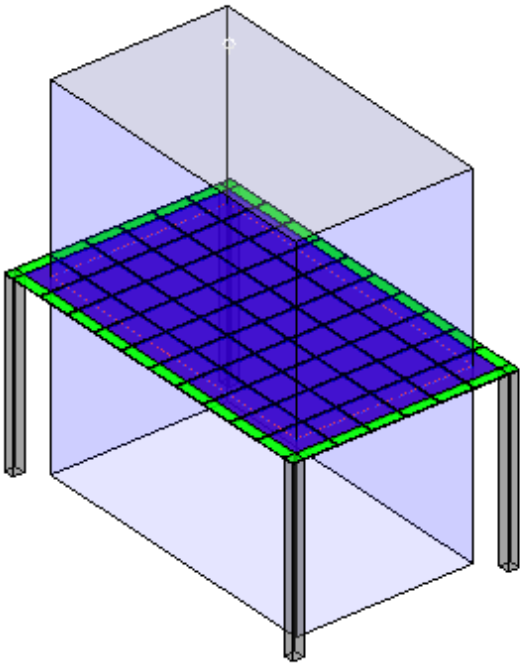

FIGURE 4.7: Monofacial flat PV module within a sandbox smaller than the PV module, generated using 'SetupBuilder'.

the following chapter. This is done in the next chapter and not in this one because the sensitivity results are integrated with irradiance meteorological data in order to calculate the final absorption value under real conditions, and therefore the difference in output value between resolution levels can be assessed in a more practical and end user oriented goal.

4.5.4 The sensitivity map for flat surfaces

In order to show visually the matrix of sensitivity output results calculated using 'SunShifter' and 'LUX', the sensitivity map is generated with the code employed by Muthukumar [32]. Figure 4.7 shows a monofacial flat PV module within a sandbox smaller than the PV module, generated using 'SetupBuilder', and Figure 4.8 shows the 10 degree sensitivity map at 600 nm for such setup simulated using 'LUX' ray tracer and 'SunShifter' to assign the correct optical properties to the different surfaces as a function of wavelength and angle of incidence, using the Cell Technology Block output, among others. Central point represents when the Sun is perpendicular to the ground. In this simulation

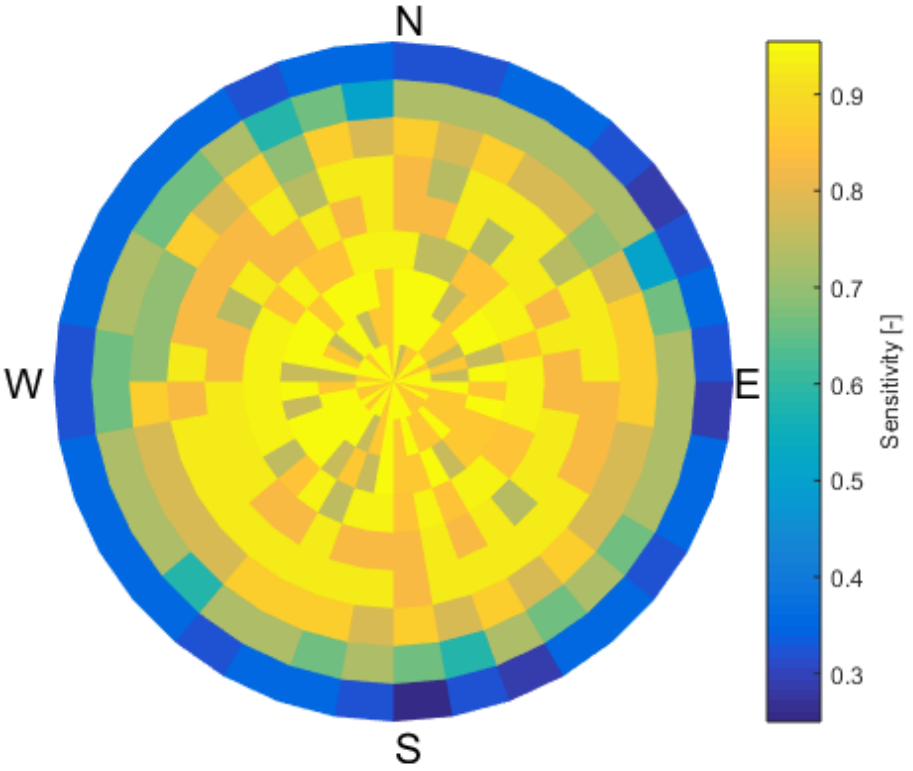

FIGURE 4.8: 10 degree resolution sensitivity map at 600 nm for a flat monofacial PV module simulated using 'LUX' ray tracer and 'SunShifter'.

10 rays are used per each run. It is observable that the module sensitivity value is 0.95 in the center of the map, as expected, and it decreases when the sun approached the horizon, down to 0.40, matching the expected values form Figure 3.9. Therefore the combination is assumed to function well for this simple design and therefore is ready to be applied to more complex structures.

4.5.5 The sensitivity map for tilted surfaces

It has to be noted that for all altitude and azimuth of incoming rays, the emitting surface is the same, the ceiling, shown in Figure 4.7. The ceiling is flat and of fixed dimensions, and thus will have a different projected area in the normal plane of the emitted light (PANPL) depending on the azimuth and altitude of the emitted rays. This projected area is relevant since it is the only area from which light will be sent. Similarly, the receiving surface, the PV cell units, also have a certain projected area on the normal plane of the incident light (PANPL). If the absorption of the PV cell units would be of 100 % for all angle of incidence, the the absorption output of the ray tracer would depend

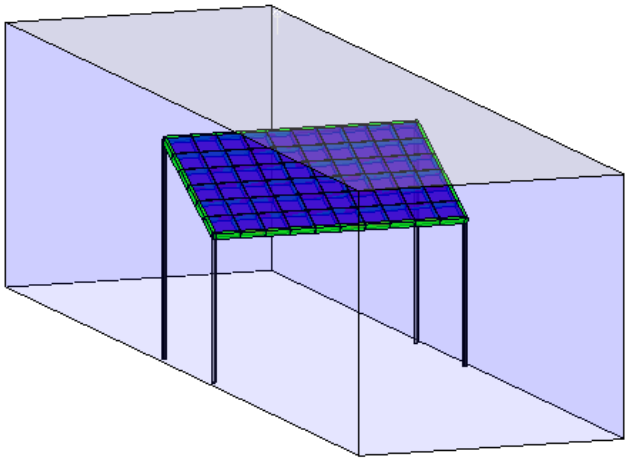

FIGURE 4.9: 27 degree tilted South facing PV module generated using 'Setup-Builder within a sandbox of 6 meter long and with the same width as the PV module.

solely on the ratio between the projected area of the PV cell units and the ceiling, shown in Equation (4.2), since it would just be a matter of how much light falls on top of the PV module and how much on the ground.

$$Ratio \quad Projected \quad Areas = \frac{Projected \quad area \quad source}{Projected \quad area \quad PV \quad module} \tag{4.2}$$

Therefore the sensitivity equation presented in Equation 4.1 can be rewritten considering the ratio of projected areas, in the manner presented in Equation 4.3.

$$Sensitivity = \frac{Light \quad intensity \quad on \quad PV \quad module}{Light \quad intensity \quad of \quad source} * \frac{Projected \quad area \quad Source}{Projected \quad area \quad PV \quad module} \tag{4.3}$$

For flat PV modules, which consequently are parallel to the ceiling, this ratio between projected areas holds the same for all altitude and azimuths, therefore the output of the ray tracer for all azimuth and altitude will be the same. The absolute value will depend on this constant value. In the case presented in the previous subsection, and shown in Figure 4.7 the ratio is always one, and thus it explains why the Sensitivity map shown Figure 4.8 is correct despite not having included this factor yet. It has to be noted that the reduced sensitivity at large angles of incidence for that sensitivity map is due to

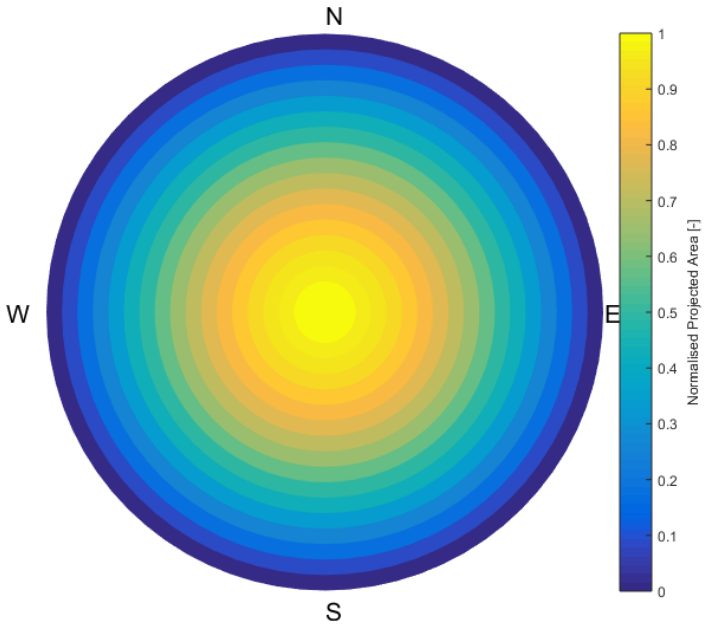

FIGURE 4.10: 5 degree resolution normalised projected area of an horizontal plane on the normal plane of the incident light, as a function of azimuth and altitude.

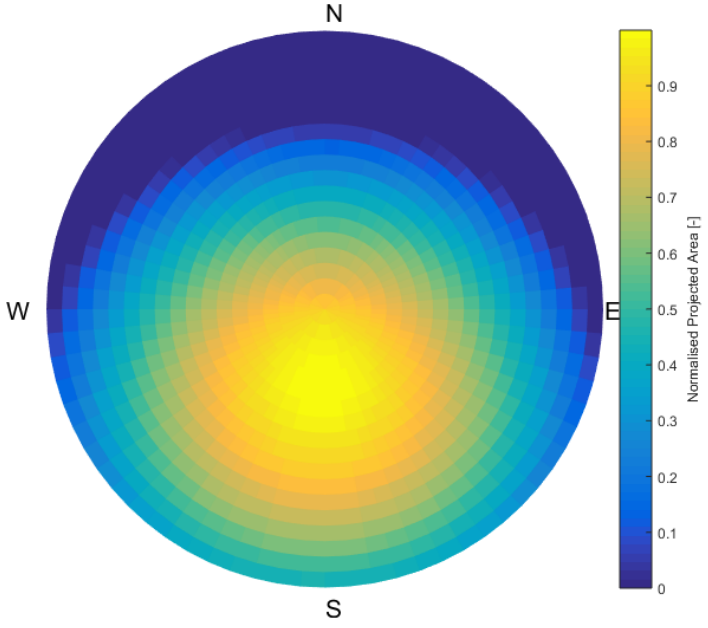

FIGURE 4.11: 5 degree resolution normalised projected area of a South facing 27 degree tilted plane on the normal plane of the incident light, as a function of azimuth and altitude.

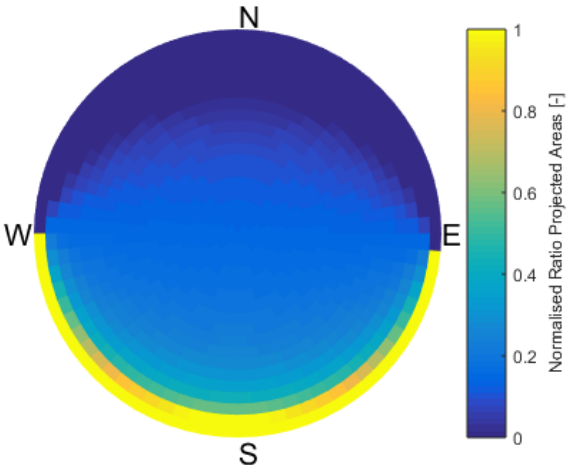

FIGURE 4.12: Normalised 5 degree resolution ratio between the normalised projected areas to the normal plane of incident light of a flat and a 27 degree South facing planes, as a function of azimuth and altitude.

a reduced absorption coefficient input employed for such angle of incidence, extracted from the cell architecture block, as explained in Figure 4.5, and not due to a difference in ratio, which, as discussed, stays constant.

For tilted PV modules, like the one shown in Figuer 4.9, however, the ratio does not stay constant. Using trigonometry, the projected area of the ceiling and the PV cell units can be found. A new Matlab function called 'AreaMatrix' is developed in order to calculate the projected area of the PV cell units and by extension its raio over the ceiling projected area. Figure 4.10 and 4.11 show the projected area of an horizontal and a South facing 27 degree tilted plane on the normal plane of the incident light, as a function of altitude and azimuth, being the center of the map when the Sun is on top of the sky. These maps represent the projected area for the ceiling, and for an example case of tilted PV module, respectively. In order to find the ratio sought in Equation (4.3), it is to be performed a right division element by element between the matrix that forms the projected PV cell map and the matrix of the projected ceiling map. Figure 4.12 show the graphic representation of the ratio between the previous two maps. If a datapoint of the the ratio results in a division by zero, the result is replaced by the next maximum non-infinite result.

Finally, the 'SunShifter' output matrix for the case represented in Figure 4.9 is shown in Figure 4.13 , where central point represents when the Sun is perpendicular to the ground. 100 rays are used per each run. It can be seen that the sensitivity between datapoints with a relative angle of incidence over the module differs, although they should hold similar values. For instance, when light is incident from the South at 66 degrees (being

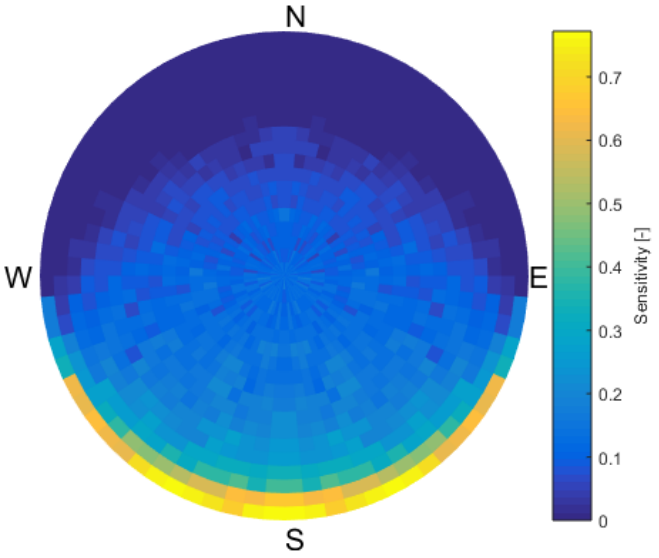

FIGURE 4.13: 5 degree resolution sensitivity map at 600 nm for a South facing 27 degrees tilted monofacial PV module simulated using 'LUX' ray tracer and 'SunShifter'.

90 degrees light coming from the horizon), the sensitivity is greater than when the light is coming form the North at 24 degrees, although the relative angle of incidence of the incoming light over the 27 degrees tilted South oriented panel is the same for both cases. This occurs because the sensitivity map has not yet been weighed over the projected area ratio as explained in Equation (4.3). Doing so, it is obtained the sensitivity map shown in Figure 4.14, which fulfills the expected sensitivity map for a PV panel at such tilt. Note that if a datapoint results in infinite due to being the value of the ratio at such incident light zero, then the value is substituted by zero, like it occurs in part of the North side of the Sensitivity map shown in Figure 4.14. Finally, it has to be noted that if the setup that has been built is symmetrical, half a Sensitivity map can be run instead and then duplicated, thus saving half of the computational time.

4.5.6 Reflector effect on sensitivity map

At this point the development of sensitivity map for PV panels placed in any kind of tilt and orientation has been discussed. The situation so far, however, has only applied to sandbox with low or no albedo, 5.6 % in the cases discussed in the previous subsections. There are situations, however, in which reflectors with great albedo, of around 80 % if white, are added, as shown in Figure 4.15. These reflectors are placed flat and contribute significantly to the generation of current since they can reflect towards the module light that would be otherwise absorbed by the ground. Therefore if the 'SunShifter' absorption

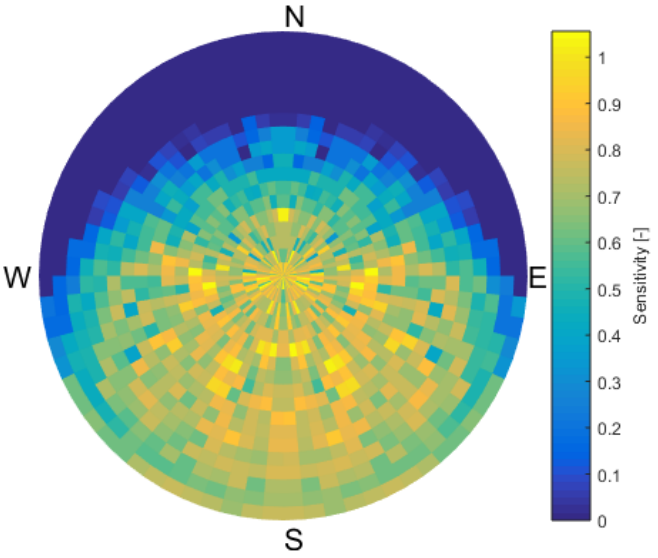

FIGURE 4.14: 5 degree resolution sensitivity map weighed over ratio between projected areas at 600 nm for a South facing 27 degrees tilted monofacial PV module simulated using 'LUX' ray tracer and 'SunShifter'.

output is weighed using Equation(4.1), the Sensitivity map will provide too high values for the datapoints in which the Sun is above the sky, since the absorption will be now high and the ratio will remain low. Therefore the area of the reflectors must be taken into account in the sensitivity equation. The reflectors are placed flat and thus will have the same normalised projection versus the incident light as the ceiling does, and which is represented in Figure 4.10. Since they contribute to current generation, their normalised projected area is added to the upper term of the ratio Equation (4.2), weighing it by their area compared to that of the ceiling and by their albedo, ending up in the form presented in Equation (4.4). If no reflectors are used but a reflective ground, then the second term of the equation is considered to be one.

Finally, it has to be noted that in order to avoid non-realistic results in case too little amount of rays is employed which is to be remembered are sent randomly, a maximum value for the sensitivity datapoints is set, equivalent to the unit plus the effective albedo on the solar module, which can be calculated for flat reflectors following the guidelines of Ziar et al. [34] using the albedo and the lenght of the reflectors as input, as well as the albedo of the rest of the ground.

$$RPA = \frac{Projected \quad area \quad source \quad + \quad Projected \quad area \quad reflectors \quad * \quad albedo}{Projected \quad area \quad PV \quad module} \tag{4.4}$$

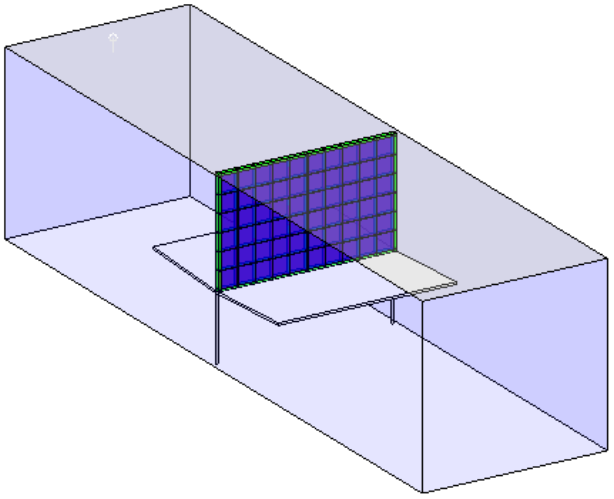

FIGURE 4.15: 90 degree tilted South facing PV module at 0.6 meter height and with 90 cm white reflectors generated using 'SetupBuilder within a sandbox of 6 meter long and with the same width as the PV module.

4.6 Application to case analysis

In this section few different setups considered for the INNOZOWA project are simulated and their sensitivity maps compared. The chosen case is to understand what is the extra gain from using reflectors and the variation due to their size.

4.6.1 Vertical setup: Reflectors vs none

In order to understand the gain produced by adding reflectors to vertical bifacial solar panels, three cases are constructed using 'SetupBuilder' and the sensitivity map generated using 'SunShifter'. The first case is vertical bifacial South facing without reflectors within a sandbox of 6 meters, distance enough to not have shade between modules when the sun is above 9.3 degrees over the horizon. This is represented in Figure 4.16. The second case, as shown in Figure 4.15, is adding 80 % albedo white reflectors of 90 cm lenght, which result in a view factor of 0.2796 and thus an effective albedo of 26.4 % considering that the ground is water with an albedo of 5.6 %. Finally, a similar third case, where the reflectors are 1.7 meter long, as shown in Figure 4.17, is also analaysed, where the view factor and the effective albedo are of 36.27 and 32.57 %, respectively.

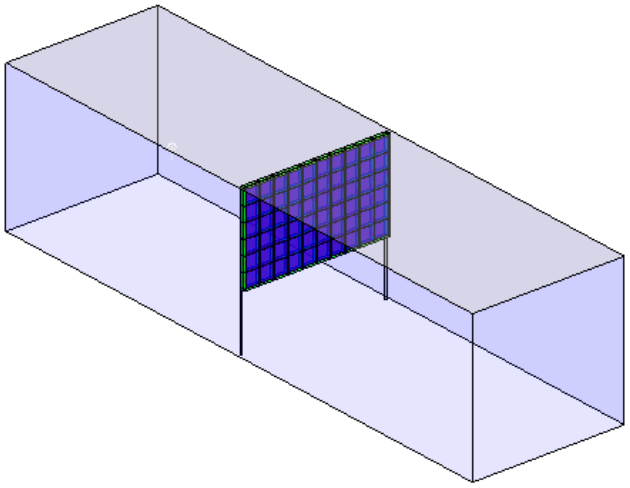

FIGURE 4.16: 90 degree tilted South facing PV module at 0.6 meter height generated using 'SetupBuilder within a sandbox of 6 meter long and with the same width as the PV module.

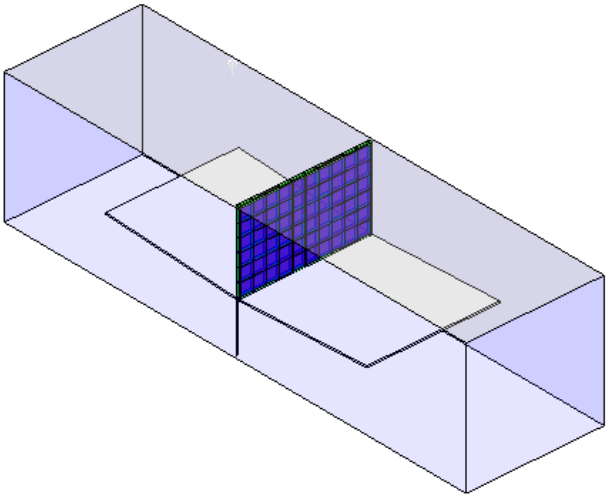

FIGURE 4.17: 90 degree tilted South facing PV module at 0.6 meter height and with 170 cm long reglectors generated using 'SetupBuilder within a sandbox of 6 meter long and with the same width as the PV module.

The corresponding sensitivity maps for the three cases are shown in Figure 4.18, 4.19 and 4.20, where 100 rays are used per each sensitivity datapoint. It can be seen that for the no reflector case, the most sensitivity datapoints are close to the horizon, when the light is almost normal to the PV module plane. For that case, on the other hand, when the Sun is close to the center of the sky not much current is generated due to the low reflecting 5.6 % reflecting ground. For the other two cases, when reflectors are added, a bigger contribution is generated when the Sun is on top of the sky, since a lot of light is incident directly on the reflectors and bounced towards the PV module. It is to be seen also that the maximum value of the sensitivity is well limited to the unit plus the effective albedo on the module, therefore the absolute light absorption value is prevented from any unrealistic value due to any overestimated sensitivity datapoint coming out form the ray-tracing. Finally, there is a common pattern in the three cases that it was not expected to occur, which is for exactly South incident light, the absorption is lower, as seen in the shape of a stripe for the three sensitivity maps. As discussed in the section 4.4.3, the sandbox represents a unit within an infinite array, thus if the azimuth of this light is quite different to the azimuth of the PV module, and light does not fall in the module the first time it goes through the sandbox, because, for instance, goes through the intercell, it is very likely that it will fall in the module on one of the following times. On the other hand, however, if the azimuth of this light is very close to the azimuth of the PV module, the light that in the first time did not fall in the cell, will keep going through the same place, for instance the intercell, and not be absorbed by the cell area. When the altitude is close to the horizon, however, light travels so many times through the sandbox that eventually gets absorbed by the cell even in such case. For higher positions of the sun, the light is bounced towards the sky if not absorbed in the first and second time that travels through the sandbox. Overall, this effect has to be taken into account when understanding the results of the integration block in which the sensitivity map is coupled with teh Sky Map.

4.7 Conclusions

This chapter has explained how to design the solar module, and the minimum volumetric replicable unit in which is found, including the most immediate shading causants, such as mounting setup and module frame. Furthermore, reflectors at the base of the modules that can reflect light into the front and rear side of a bifacial module also have been replicated. To do so, a program called 'SetupBuilder' using the 'Lux' environment has been developed to provide the base and flexibility to build the aforementioned components. 'LUX' operation consists of four main steps: the creation of the vertex found

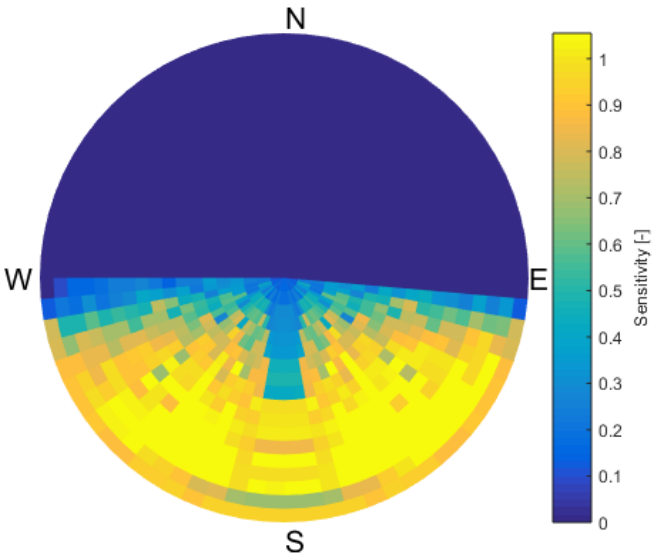

FIGURE 4.18: 5 degree resolution sensitivity map weighed over ratio between projected areas at 600 nm for a South facing 90 degrees tilted PV module without reflectors simulated using 'LUX' ray tracer and 'SunShifter'.

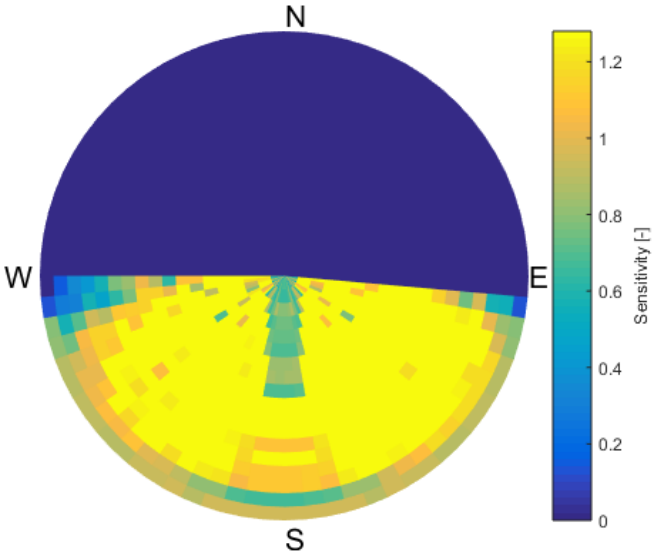

FIGURE 4.19: 5 degree resolution sensitivity map weighed over ratio between projected areas at 600 nm for a South facing 90 degrees tilted PV module with 90 cm flat white reflectors simulated using 'LUX' ray tracer and 'SunShifter'.

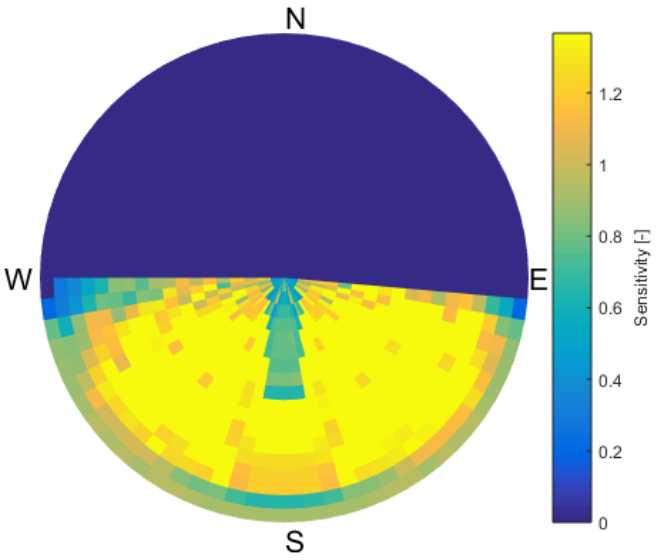

FIGURE 4.20: 5 degree resolution sensitivity map weighed over ratio between projected areas at 600 nm for a South facing 90 degrees tilted PV module with 170 cm flat white reflectors simulated using 'LUX' ray tracer and 'SunShifter'.

in the setup; the joining of facets, either quadrangular or triangular, using those vertex as reference; the allocation of material properties at each side of every facet, and the wavelenght of light that is desired to trace. 'SetupBuilder' has been designed to provide control to the different dimensions of cells, as well as the ability of decided amount of cells per row and column of the module. Also it is possible to state the tilt angle and orientation of the module. Finally, the coded is suited to replicate the module along different rows and columns, in order to simulate the conditions of a PV field. The output of the Lux program is given as the amount of light absorbed per each surface depending of the direction of the incident light, and therefore the amount of photons per each cell on front and rear side, separately, can be analyzed. Using this output, a sensitivity map for every wavelength, based on V. Muthukumar concept, and adjusted in this chapter depending on the tilt of the PV module and the addition of reflectors, can be extracted for front and for rear side, as a function of the angle of incidence and azimuth of the incoming light, taking into account every spectral and angular depending change in the cell absorption value predicted by the Cell Technology Block.

An analysis of necessary number of rays to obtain accurate results has been performed and it is found that in order to reproduce PV modules that are at a PV farm like front distance from each other, of around 6 meters, and a side distance equivalent to the lenght of the module. 1000 rays per sensitivity datapoint provide a standard deviation of 0.02 over the absolute value, which is considered reasonable. It is also found that the sensitivity maps held expected values, although for the vertical situations there is

a small decrease in absorption for light incident from the very same azimuth as the one the module is oriented, the impact of which will be assessed in the next Chapter. Finally, the example of three different vertical bifacial PV modules with and without reflectors has been analysed, and it is seen that the reflectors contribute to a better gain in absorption for situations in which the sun is closer to the zenith, compared to a more South low altitude receptive sensitivity map when no reflectors are added. It is also seen that an increment of almost double the lenght in reflector, form 90 to 170 cm, yields little increment in the absolute value of the sensitivity map, and does not change its distribution.

Chapter 5

Location Integration Block

In the technology chapter, the light absorption of a certain technology is assessed as a function of wavelength and angle of incidence. Additionally, in the PV system design chapter the influence of the surroundings of the cell on the incident irradiance are considered. The present chapter aims to integrate the output of both chapters together with a sky model based on actual meteorological data in order to predict irradiance absorbed by the PV module over a period of time and by extension the current generated. Afterwards, a selected thermal model is also added. Finally, the explanation on how to assess the single diode characteristics at different irradiances and temperatures is also assessed in order to integrate the electrical model.

5.1 Concept, input and output of the Optical part

The integration block aims to predict the irradiance absorbed by a PV panel and by the cSi layer over a period of time. The input are therefore the historical irradiance data for a given location, the sensitivity map for a chosen 3D setup and cell technology, and the ratio between cSi and PV module absorption as a function of wavelength, since, as shown in Figure 3.10 it does not change over angle of incidence. Regarding the irradiance data, some sources provide either the Global Horizontal Irradiiance (GHI) or a breakdown of it in Diffuse Horizontal Irradiance (DHI) and Direct Normal Irradiance (DNI). If it is the first case, then a decomposition model must be applied. Once the DHI and DNI values are known, a Sky Map showing the amount of light per every azimuth and altitude of the hemisphere is constructed. To do so, the model developed by Muthukumar is applied [32]. This Sky Map can be later integrated together with

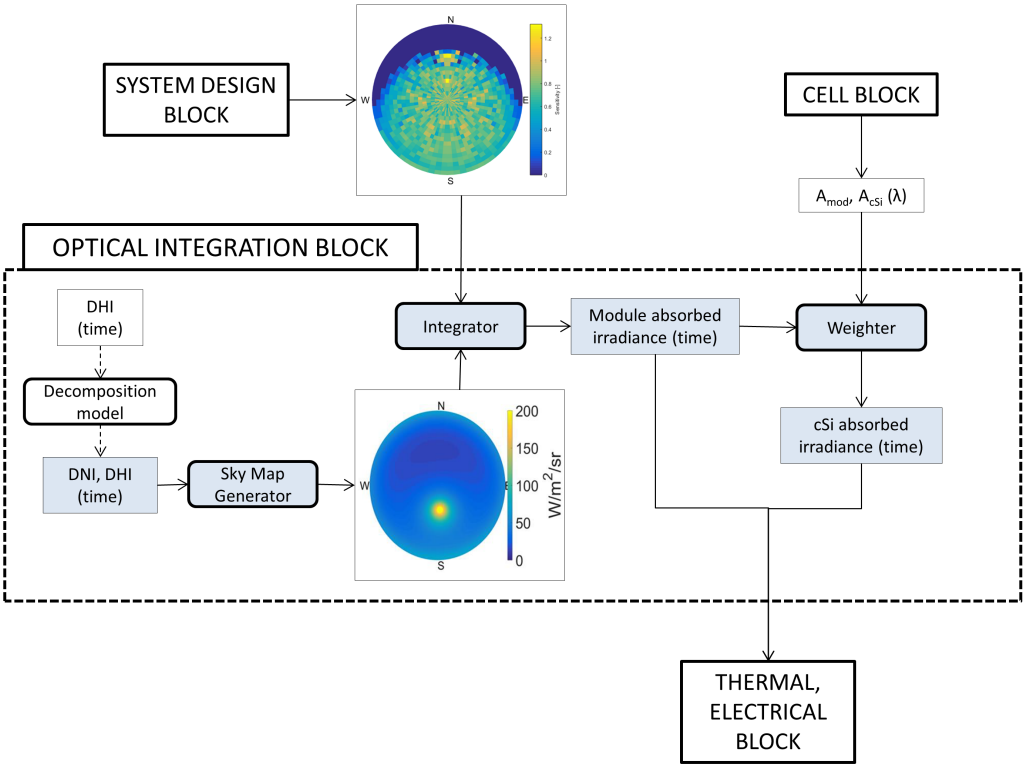

FIGURE 5.1: Algorithm of the Optical Integration Block. Dashed lines represent features that are not hard-coded in the current version toolbox.

the Sensitivity Map and therefore the total absorption of the PV module calculated. Finally this absorption is weighed with the cSi and PV module absorption ratio in order to estimate the genartion of current by the PV module.

Figure 5.1 shows the approach discussed and employed in this thesis work. As it is indicated in the figure, the decomposition model is left out of the input. This is due to the meteorological source employed, Meteonorm, which already provides the DNI and DHI data.

5.2 Generation of Sky Map

At every unit of time, the incident light from every point of the sky needs to be known in order to understand what share of it can be absorbed by the PV modules. To do so, the light from every In order to The DNI and DHI values are distributed through the skyk following the Perez model explained by Muthukumar [32]. Figure 5.2 shows a Sky Map for an entire year for the location of Weurt, in The Netherlands, with a resolution

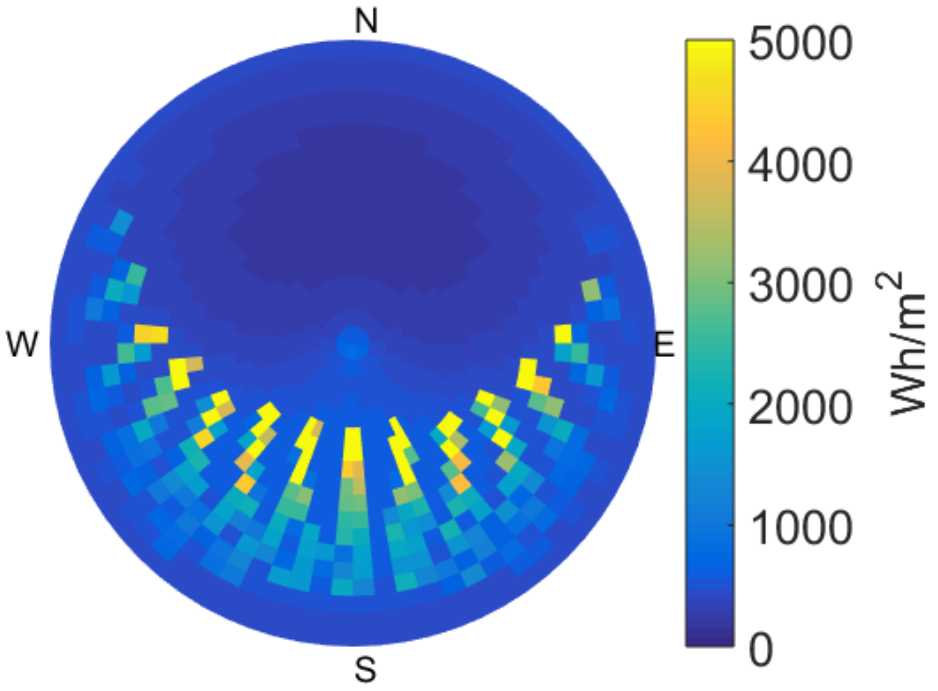

FIGURE 5.2: Sky Map with 5 degree resolution for an entire year for the location of Weurt, in The Netherlands

of 5 degrees. Integrating the entire Sky Map it can be seen that the annual irradiance for such location is of 967 kWh/m2, which is in line with the expected annual irradiance for The Netherlands.

5.3 Integration with Sensitivity Map

This Sky Map is multiplied point by point with the Sensitivity Map in order to determine how much power is absorbed by the Solar PV panel. When integrating the Sky Map presented in Figure 5.2 and the Sensitivity Map presented in Figure 4.11, it can be seen that the irradiance received by the PV panel is of 663 kWh/m2. Weighing it over the cSi layer versus module absorption ratio determined in the Cell Technology and the 3D Setup System blocks, the cSi layer absorbs 621 kWh/m2. Figure 5.3 shows the GHI, DNI and DHI for the Weurt location for an entire year, as a function of hour. ONly hours in which the SUn is above the horizon are considered. The module and cSi power absorption is also shown.

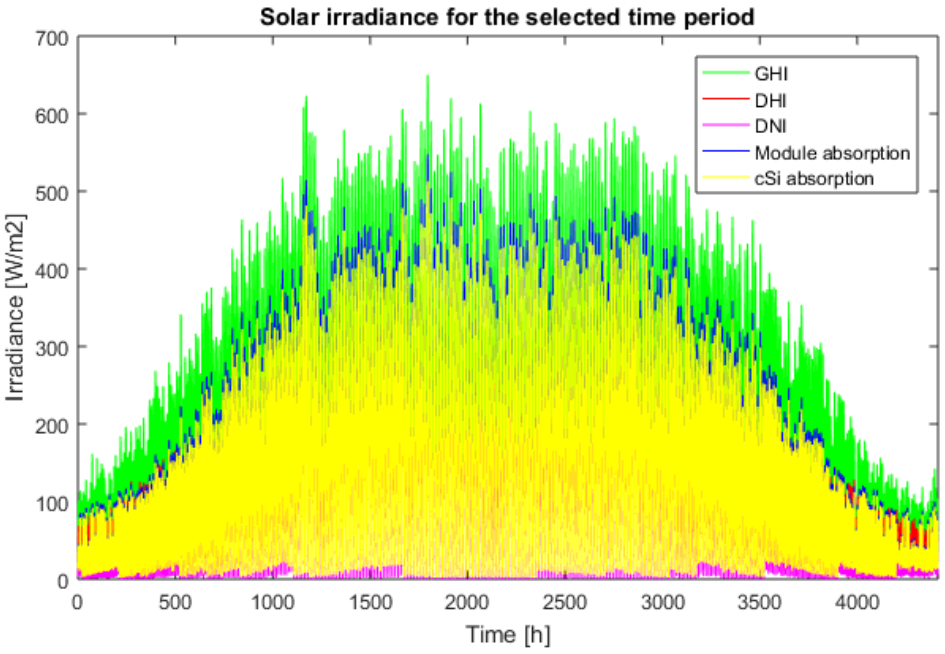

FIGURE 5.3: Annual Global, Direct and Diffuse Irradiance for the location of Weurt in The Netherlands. Power absorption by the module and the cSi layer for a 27 degrees tilted PV panel is also shown.

5.4 Integration of Thermal part

Afterwards, the thermal block has the aim of accurately predicting the operating cell temperature at every moment. To develop such a task several meterological data input such as wind speed and ambient temperature is needed. Besides, the irradiance on the plane of array, which is the output of the optical block, also influences the cell temperature. Finally, certain cell technology parameters such as the temperature coefficients, which are an output of the technology block, are also to be known in order to calculate the electrical power flux flowing through the cell, which also affect the cell temperature.

The modifyied fluid dynamics model developed by Faturrochman [42] is coded within the Toolbox. This approach makes use of the ambient temperature, wind speed and front and rear irradiance. Using these changing values per hour as input, the cell temperature is calculated per every unit of time, as shown in Figure 5.4. It can be seen that besides increasing together with ambient temperature, the module temperature also increases significantly in summer periods when the absorbed irradiance by the PV cell is larger.

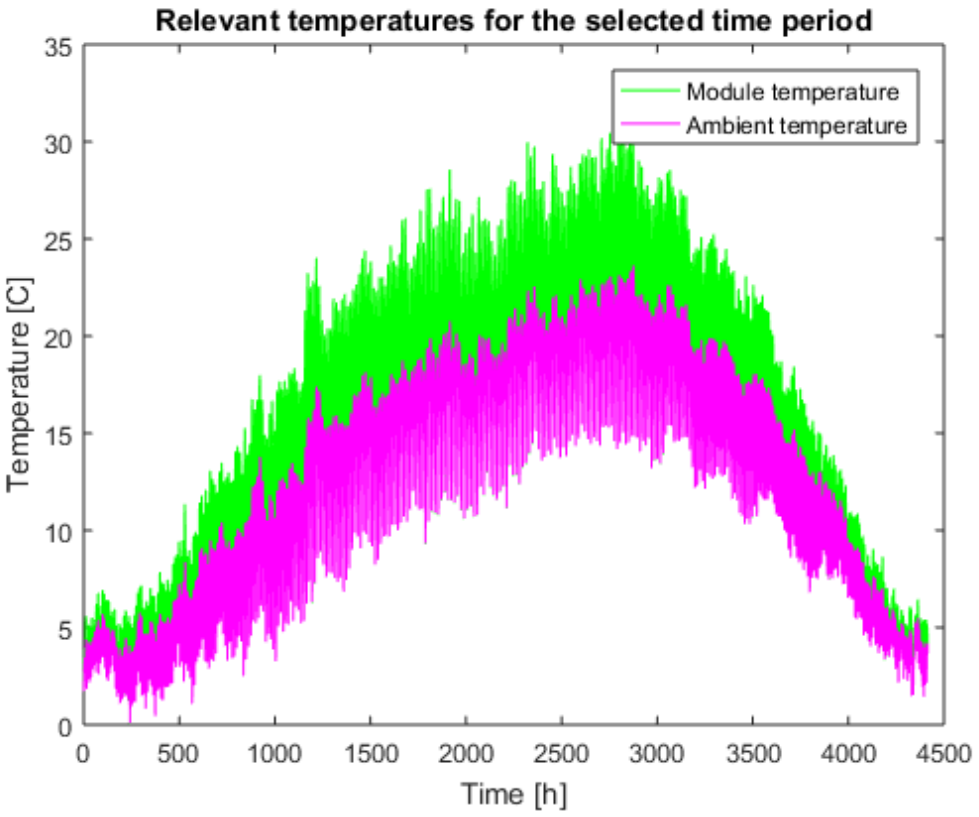

FIGURE 5.4: Annual ambient and module temperature for the location of Weurt in The Netherlands.

5.5 Electrical part approach and algorithm

The electrical block has the goal of accurately assessing how much electricity can be extracted out of the PV module at every point of time. The required input for such module is the absorbed light in the cell, which depends on the irradiance at the plane of array, the electrical parameters of the technology block, which give information on how much current is absorbed under certain irradiance at standard test conditions, and the temperature coefficients to know how these parameters change with temperature. Finally, the cell temperature is also needed. Once irradiance on the plane of array, cell temperature and IV curve at STC conditions is known, an algorithm shall be developed such that finds the five single diode parameters at that irradiance and temperature and consequently can develop the IV curve under those conditions.

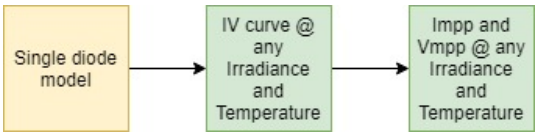

FIGURE 5.5: Electrical model algorithm desired output (1/4).

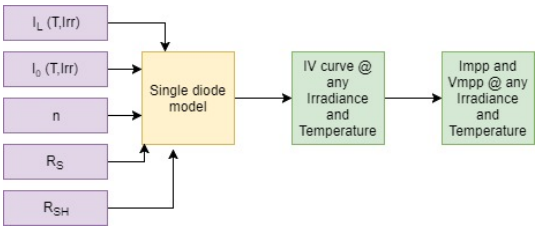

FIGURE 5.6: Electrical part algorithm desired output (2/4).

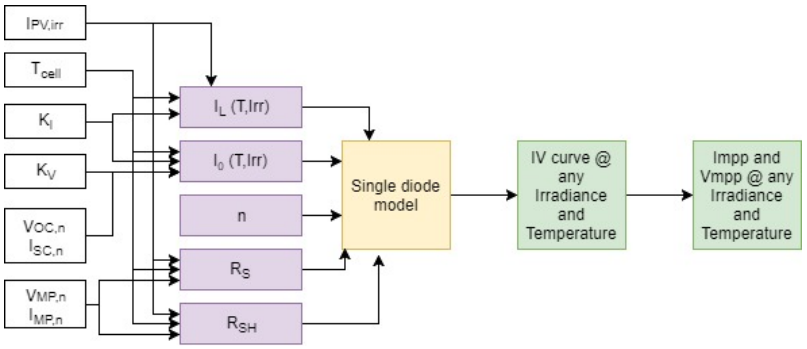

FIGURE 5.7: Electrical model algorithm desired output (3/4).

5.5.1 The evolved single-diode model

As seen in the literature review, the single diode model requires five parameters to generate IV curves. These parameters rely at the same time on other input such as cell temperature, and Voc, Isc, Vmpp and Impp at nominal conditions. The get together of all this parameters in a efficient manner is developed in this chapter

5.6 Solution at Standard Test Conditions

The task of making an algorithm is no trivial one. The first step is to define the end goal of the algorithm. In this case, to obtain the Impp and Vmpp at any irradiance and temperature operating conditions. For such purpose the IV curve of the module at such conditions needs to be modelled. Therefore this is the end goal, as represented in Figure 5.5.

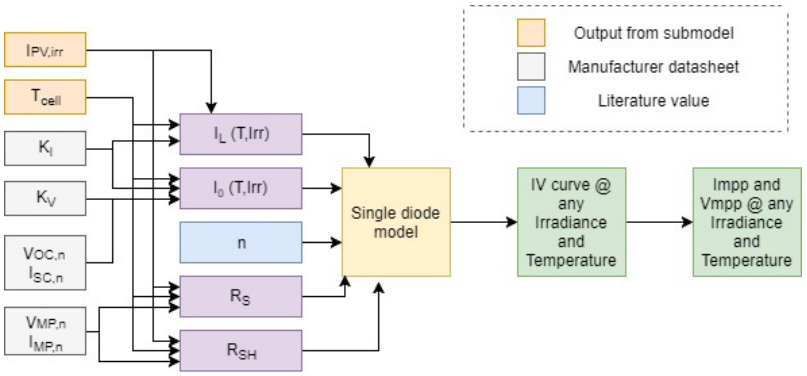

FIGURE 5.8: Electrical model algorithm desired output (4/4).

Now it is time for defining what input is needed to get to such end goal. As defined before, the five single diode parameters are needed for such purpose. It is worth to distinguish them between those that vary with temperature and irradiance and those which do not. Rs, Rsh and n, as explained in the literature review, do not. Il and I0 on the other hand, do. Thus the algorithm becomes as the one depicted in Figure 5.6.

The next step is to find out which ones of the inputs are readily available and which ones require extra steps. As found out in literature, Il depends on the Ipv at nominal conditions (Ipv,n), which are 25 C and 1000 W/m2, and of the current temperature coefficient and the updated irradiance and temperature conditions. The toolbox presented in this Thesis, however, can accuratelly provide the absorbed Ipv at any level of irradiance, and thus the formula from Equation (2.16) is updated to the following Equation (5.1). On the other hand, J0 depends on Isc and Voc at nominal conditions, the cell temperature and the temperature coefficients, as shown in Equation (2.19). Finally, the ideallity constant n can be found in literature, and Rs and Rsh are calculated using Impp, Vmpp, Isc and Voc at nominal conditions. Therefore the algorithm evolves to the one shown in Figure 5.7.

$$I_{PV} = (I_{PV,irr} + K_I \Delta_T) \tag{5.1}$$

Finally, the last step is to identify where these input can be taken from. Obviously Ipv,irr is the ouput from the optical block of this toolbox, also known as optical absorption. The Tcell is the output of the thermal model, which is defined in the following section. The temperature coefficients and nominal Isc, Voc, Impp and Vmpp are taken from the manufacturer datasheet. Lastly, the ideality factor n is taken form literature. Therefore three sources are identified, output from submodels, literature and manufacturer datasheet. This is summarized in Figure 5.8. It is to be noted however that given

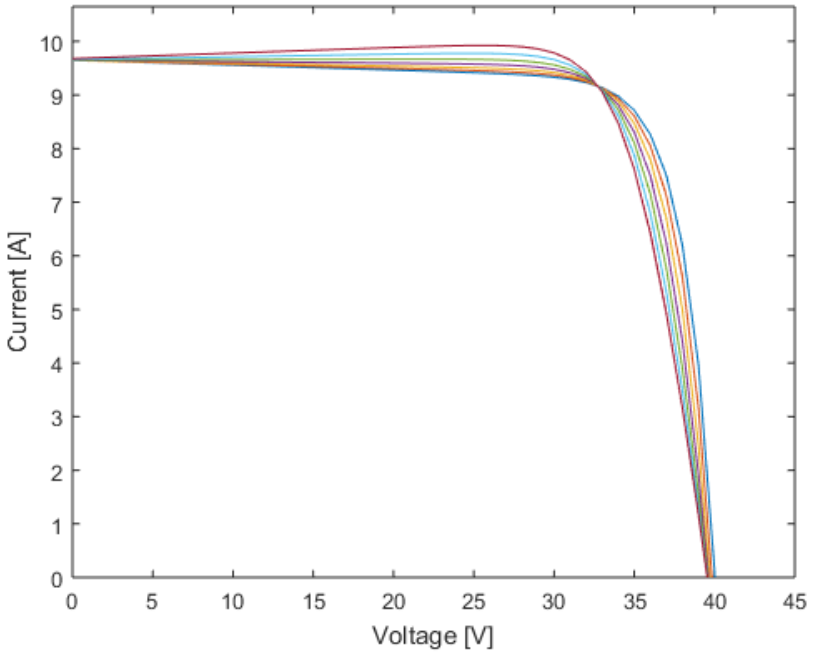

FIGURE 5.9: IV curves with the same Voc, Isc and with different pairs of Rs and Rsh values.

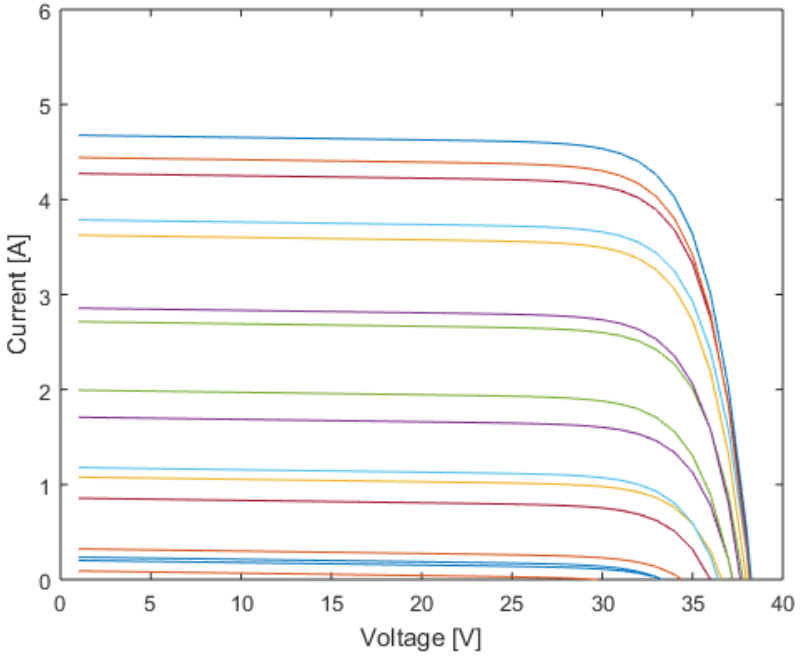

FIGURE 5.10: IV curves at different times of the day for a 27 degree tilted PV module for the location of Weurt in The Netherlands.

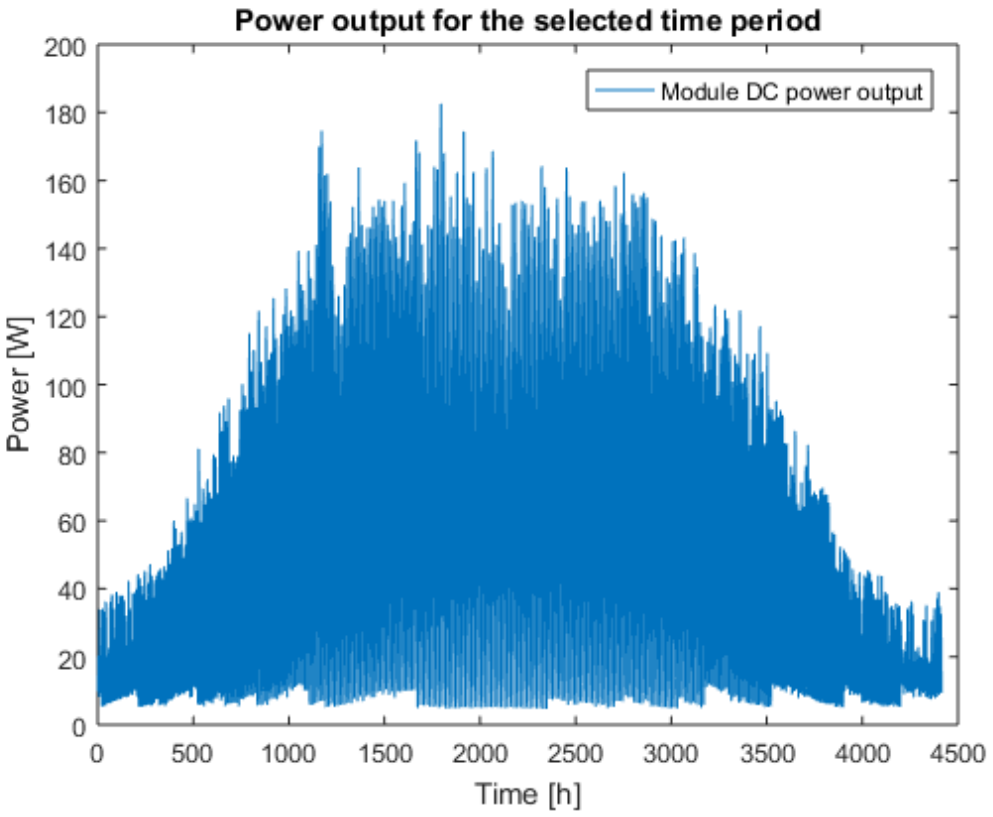

FIGURE 5.11: Annual DC Power Output for the location of Weurt in The Netherlands.

that the architecture of the cell is input during the optical model, some parameters such as Voc, Isc, Vmpp and Impp could be estimated from that chapter. This is however, a piece of research that can be implemented in future work.

As Villalva suggests [46], to find Rs and Rsh it is necessary to iterate until the Pmax,n is matched. It is suggested that Rs is slowly incremented starting form Rs = 0. Therefore the first step in the code of the bifacial toolbox is to find out the corresponding Rsh when Rs = 0. Afterwards, the full IV curve is computed and it is checked whether the Pmax of the modelled curve matches the experimental Pmax. If not, Rs is slowly incremented and Rsh computed again and so the procedure is repeated. Figure 5.9 illustartes this visually.

5.7 Parameters at different temperature and irradiance

For different temperatures, the saturation current has to be calculated. This is done by calculating the new saturation current via Equation (2.19). The rest of parameters such

as shunt, series resistance and ideality factor are kept the same. The photogenerated current will be directly proportional to the irradiance absorbed by the PV cell. Therefore IV curves for different times of the day can be calcultaed, as shown in Figure 5.10 for a day in July at the location of Weurt.

5.8 Integration of the Electrical part and DC yield of case analysis

Once the electrical model is able to generate IV curves at any given temperature and irradiance and thus short-circuit current, the electrical model is integrated with the output of the optical and thermal model. For the output of the optical model, the absorbed power is weighed by the current generation of the solar spectrum in the range of 300 to 1200 nm, which is of 46.46 mA/cm2. Therefore, the short-circuit current of each cell can be calculated knowing its area of 15.675 per 15.675 cm. Other relevant electrical parameters of the PV panel are taken from the datasheet. Using the electrical model, the DC power generation of the PV panel is presented in Figure 5.11. Integrating fro the entire year, it can be seen that the PV panel generates 238 kWh annualy.

Chapter 6

Overall conclusions and Recommendations

6.1 Conclusions on the Goals

The work presented in this Thesis has developed a comprehensive cell to annual energy yield model that can carry out annual energy prediction for innovative PV installations such as floating PV Systems. The achievement of the subgoals within these goals are discussed in the following subsections.

6.1.1 Goal 1: To build a modular AEY bifacial toolbox

- Goal 1: To build a modular AEY bifacial toolbox: A modular approach to modelling the performance of bifacial PV panels has been developed. The real PV module installation has been decoupled in three blocks: Cell Technology Block, System Setup Block and Location Integration Block, where the later is composed of Sky, Thermal and Electrical models.
  - Subgoal 1.1: Identify best match of PVMD models: It has been found that for predicting cell absorption properties, the GenPro4 wave and ray optics can accuratelly assess it as a function of wavelength and angle of incidence. For determining c-Si layer current generation, the method that couples a Sensitivity Map with a Sky Map has been applied. For the Thermal model, the Fluid Dynamics Bifacial model has been found as an excellent match.

- Subgoal 1.2: Develop missing pieces: Regarding ability to construct 3D setup, a Matlab code has been developed which can reproduce geometrical input regarding PV module, mounting structure, ground and reflectors, and assign optical properties to it as a function of wavelength and angle of incidence. For bifacial modules, the absorption value input for the rear side is the average over all angle of incidences, since most of the contribution to current generation is due to diffuse light. Regarding the Sensitivity Map generation, it has been found that ratio between the projections of the emitting and receiving surfaces on the normal plane of the incident light plays a role, and an approach to correct for it has been developed. Finally, an Electrical model aapproach to obtain the IV curve at any given point of time, considering the module temperature and current generated has been developed.
- Subgoal 1.3: Integrate and assess accuracy: It has been determined that at for the Cell Technology Block, the best practices are found to perform, simulations with 100 rays, every 100 nm wavelenght and a set of 9 simulations per wavelength at different angle of incidence. Using these parameters, the cell and c-Si layer absorption values yield a standard deviation of $\pm$ 0.4% and 0.8%, respectively. As for the System Setup Block, the standard deviation of the sensitivity values generated depends on the relative area between the sandbox and the PV panel within it, although for environments with a distance between rows close of 3 meters, close to usual practices, 1000 rays per simulation are enough to get an standard error of $\pm$ 2.0 % per Sensitivity datapoint.

6.1.2 Goal 2: To apply it to optimize design of a real case

- Goal 2: To optimize design of a real floating PV case: Optimization for the best techonology and design choice for the floating PV device within the INNOZOWA project has been carried out and the Annual Energy Yield estimation performed for one of the technologies and design.
  - Subgoal 2.1: Account for angle of incidence and spectral effects: The optical properties of a monofacial versus a bifacial cell, including EVA and glass layers, has been assessed, observing an immediate current generation gain of 1.44 % more current for the monofacial, since bifacial transmits more light. However this light transmission is later accounted for within the Sensitivity Map calculation, as it can be reflected back to the module.

- Subgoal 2.2: Reproduce complex design: The two designs considered during the development of the INNOZOWA project, tilted monofacial over water and vertical bifacial with reflectors have been succesfully reproduced with the System Setup Block, including mounting structure.
- Subgoal 2.3: Account for bifaciality and albedo gains: The Sensitivity Map of four different designs involving monofacial tilted and vertical bifacial panels with reflectors of different sizes have been generated. It is seen that how for the vertical bifacial cases, the reflectors shift the Sensitivity of the setup towards light incident for greater altitude.

6.2 Recommendations

For future work, the most relevant and immediate point of interest as identified by the author is:

- The experimental validation of this toolbox as a whole against outdoor field data. Although the different models have been validated separately, the Sensitivity Map translation from LUX ray tracer output has not been validated yet, and can influence the match of the entire Toolbox output versus real situations.

Besides this point that is key in order to make the Toolbox publicly available, there are other improvements that can elevate the quality of the toolbox:

- In the same manner the cell absorption is input as a function of AOI and wavelength when calculating the Sensitivity Map, the same should be possible for ground and reflector albedo. Therefore coding this possibility will enhance the accuracy of the toolbox.
- The consideration of inter-row shading for PV farm setup, since the current LUX ray-tracing system accounts the light absorbed by the nearby modules as if it was absorbed by a single unit.
- Adding the feature of generating a separate Sensitivity Map per every cell to understand better any bypass diode effect when partial shading occurs.
- The integration of the Horicatcher tool in the Sensitivity map which can account for far horizon optical loses.

- Further work on the 'SetupBuilder', in order to be able to generate other shapes such as curved PV modules or reflectors underneath a flat PV panel, will also add versatility to the toolbox.
- Research on the generation of Sensitivity Map for even more complex setups, considering the role that the different projected areas pay on this item.
- Finally, the integration of alternative models for each of the blocks also has to be considered, as different models have different advantages and for the moment the toolbox only offers one model per each block.

Acknowledgements

To Rudi: Thanks for faithfully sharing this journey with me, your knowledge and humanity has made it certainly a pleasant one. To Olindo and Arno: Your dedication to this group is exemplary, it is an honour to develop my academic career under your supervision. To Hesan: Your help with Innozowa has been crucial, I appreciate it. To the Eternal Sun team: I have the opportunity to travel the world and meet, present and discuss with the most brilliant minds of the PV family thanks to the trust you put on me. We make a great match. To Vimanyu, Vitesh and Prashant: You are literally my family in the Netherlands. If anybody embodies the legendary warmth of Indian hospitality that is you. Yahan Ke Hum Sikandar. To my friend Ibra: you are the spark that started everything, and loyaly remain by my side, I thank you for that. To my friend Mike: your life philosophy is admirable, it makes me grow as a person, and that is pretty cool. To Anne: You are the icing of the cake, surely life has great things ready for us. To all the wonderful people I have met during my adventures in Delft and in London: Keep making this a better world, from whatever corner of the globe you are based now.

To my Mom and Dad: Gracies per donar-me la oportunitat, us estimo.

Va per tu Gabri,

Bibliography

[1] P. Earis, "Balancing scales," *Joule*, vol. 1, no. 2, pp. 201 – 203, 2017.

[2] "Production modeling for grid-tied pv systems: Page 12 of 14 — solarpro magazine." http://solarprofessional.com/articles/design-installation/production-modeling-for-grid-tied-pv-systems/page/0/11#.WeSU9Pl95pg. (Accessed on 10/16/2017).

[3] "Ludzidzi zwane — professional profile." https://www.linkedin.com/in/ludzidzi-zwane-28017137. (Accessed on 16/10/2017).

[4] Sol-Up, "Henderson solar panel installation." http://www.solup.com/henderson-solar-panel-installation. (Accessed on 14/04/2018).

[5] A. Jones and C. Underwood, "A thermal model for photovoltaic systems," *Solar Energy*, vol. 70, no. 4, pp. 349 – 359, 2001.

[6] J. A. Eikelboom and A. Reinders, "Determination of the irradiation dependent efficiency of multicrystalline Si PV modules on basis of IV curve fitting and its influence on the annual performance," *Measurement*, pp. 2–5, 1997.

[7] M. Boccard, "Silicon-based heterojunction solar cells." https://pvlab.epfl.ch/heterojunction_solar_cells. (Accessed on 28/02/2018).

[8] C. Honsberg and S. Bowden, "Surface Texturing," 2018.

[9] A. Becquerel, "Memoire sur les effects delectriques produits sous linfluence des rayons solaires," *Annalen der Physick und Chemie*, vol. 54, pp. 35–42, 1841. ¡br /¿.

[10] R. Ohl, "Light-sensitive electric device," June 25 1946. US Patent 2,402,662.

[11] D. M. Chapin, C. S. Fuller, and G. L. Pearson, "A new silicon pn junction photocell for converting solar radiation into electrical power," *Journal of Applied Physics*, vol. 25, no. 5, pp. 676–677, 1954.

[12] S. DeWolf, A. Descoeudres, Z. Holman, and C. Ballif, "High-efficiency silicon heterojunction solar cells: A review," *Green*, vol. 2, no. 1, pp. 7–24, 2012.

[13] M. A. Green, Y. Hishikawa, W. Warta, E. D. Dunlop, D. H. Levi, J. Hohl-Ebinger, and A. W. Ho-Baillie, "Solar cell efficiency tables (version 50)," *Progress in Photovoltaics: Research and Applications*, vol. 25, no. 7, pp. 668–676, 2017. PIP-17-089.

[14] W. Shockley and H. J. Queisser, "Detailed balance limit of efficiency of p-n junction solar cells," *Journal of Applied Physics*, vol. 32, no. 3, pp. 510–519, 1961.

[15] J. Olson, S. Kurtz, and D. Friedman, "Multi-junction, monolithic solar cell using low-band-gap materials lattice matched to gaas or ge," Aug. 28 2001. US Patent 6,281,426.

[16] I. Haedrich, M. Wiese, B. Thaidigsman, D. Eberlein, F. Clement, U. Eitner, R. Preu, and H. Wirth, "Minimizing the optical cell-to-module losses for mwt-modules," *Energy Procedia*, vol. 38, no. Supplement C, pp. 355 – 361, 2013. Proceedings of the 3rd International Conference on Crystalline Silicon Photovoltaics (SiliconPV 2013).

[17] ITRPV, "International Technology Roadmap for Photovoltaics (ITRPV) Results 2016," tech. rep., 2017.

[18] Yingli Solar, *Panda Bifacial 60CF*, May 2017.

[19] ECN, "Ultrasimple process for mass production of ibc silicon solar cells," Apr. 4 2017. https://www.ecn.nl/news/item/ultrasimple-process-for-mass-production-of-ibc-silicon-solar-cells/.

[20] R. Kopecek, "Bifaciality: still an advantage for n-type?." SiliconPV 2017.

[21] "index." http://www.steveransome.com/. (Accessed on 10/16/2017).

[22] PVsyst SA, "Pvsyst6 photovoltaic software," Oct. 16 2017. https://sam.nrel.gov/.

[23] PVsyst SA, "Detailed electrical losses," Oct. 15 2017. http://files.pvsyst.com/help/bifacial_systems.htm.

[24] PVsyst SA, "Bifacial systems," Oct. 15 2017. http://files.pvsyst.com/help/near_shadings_electrical.htm.

[25] F. Sonmez Master's thesis, Technical University of Delft, Photovoltaic Devices and Materials Group, November 2017.

[26] *5CO.7.1 Light Induced Degradation of Rear Passivated mc-Si Solar Cells*, 33rd European Photovoltaic Solar Energy Conference and Exhibition, Sept. 27 2017.

[27] F-Chart Software, "Pv f-chart," Oct. 16 2017. http://www.pvsyst.com/en/.

[28] NREL, "System advisory model (sam)," Oct. 16 2017. http://www.fchart.com/pvfchart/.

[29] Fraunhofer, "Smartcalc.ctm," Oct. 15 2017. https://www.cell-to-module.com/software/features.

[30] R. Santbergen, T. Meguro, T. Suezaki, G. Koizumi, K. Yamamoto, and M. Zeman, "Genpro4 optical model for solar cell simulation and its application to multijunction solar cells," vol. PP, pp. 1–8, 03 2017.

[31] R. Santbergen, R. Mishima, T. Meguro, T. Suezaki, M. Hino, H. Uzu, G. Koizumi, J. Blanker, K. Yamamoto, and M. Zeman, "Optical simulation of multi-junction solar cells," 01 2016.

[32] R. Santbergen, V. Muthukumar, R. Valckenborg, W. van de Wall, A. Smets, and M. Zeman, "Calculation of irradiance distribution on pv modules by combining sky and sensitivity maps," vol. 150, pp. 49–54, 07 2017.

[33] G. Faturrochman, M. de Jong, R. Santbergen, W. Folkerts, M. Zeman, and A. Smets, "Maximizing annual yield of bifacial photovoltaic noise barriers," vol. 162, pp. 300–305, 03 2018.

[34] H. Ziar, B. Asaei, S. Farhangi, M. Korevaar, O. Isabella, and M. Zeman, "Quantification of shading tolerability for photovoltaic modules," vol. PP, pp. 1–10, 07 2017.

[35] J. Stultz and J. Kratochvil, "Thermal performance testing and analysis of photovoltaic modules in natural sunlight," *DOE/JPL LSA task report 5101-31*, 1977.

[36] O. Isabella, K. Jäger, A. Smets, R. van Swaaij, and M. Zeman, *Solar Energy: The physics and engineering of photovoltaic conversion, technologies and systems*. UIT Cambridge Limited, 2016.

[37] P. Trinuruk, C. Sorapipatana, and D. Chenvidhya, "Estimating operating cell temperature of bipv modules in thailand," *Renewable Energy*, vol. 34, no. 11, pp. 2515 – 2523, 2009.

[38] J. A. Duffie and W. A. Beckman, *Solar Engineering of Thermal Processes, 4th Ed.* Wiley, 2016.

[39] A. Jamodkar, "Energy yield prediction of solar powered e-bike charging station," Master's thesis, Technical University of Delft, Photovoltaic Devices and Materials Group, July 2017.

[40] M. Fuentes, "A simplified thermal model for flat-plate photovoltaic arrays," 05 1987.

[41] G. Notton, C. Cristofari, M. Mattei, and P. Poggi, "Modelling of a double-glass photovoltaic module using finite differences," *Applied Thermal Engineering*, vol. 25, no. 17, pp. 2854 – 2877, 2005.

[42] G. J. Faturrochman, "Design optimization of bifacial photovoltaic noise barriers using a high granularity energy yield modelling approach," Master's thesis, Technical University of Delft, Photovoltaic Devices and Materials Group, July 2017.

[43] H. Tian, F. Mancilla-David, K. Ellis, E. Muljadi, and P. Jenkins, "A cell-to-module-to-array detailed model for photovoltaic panels," *Solar Energy*, vol. 86, no. 9, pp. 2695 – 2706, 2012.

[44] C. Vimalarani and N. Kamaraj, "Modeling and performance analysis of the solar photovoltaic cell model using embedded matlab," *SIMULATION*, vol. 91, no. 3, pp. 217–232, 2015.

[45] E. Meyer, "Extraction of saturation current and ideality factor from measuring voc and isc of photovoltaic modules," *International Journal of Photoenergy*, vol. 2017, p. 9, 2017.

[46] M. G. Villalva, J. R. Gazoli, and E. Ruppert Filho, "Comprehensive approach to modeling and simulation of photovoltaic arrays," *IEEE Transactions on power electronics*, vol. 24, no. 5, pp. 1198–1208, 2009.

[47] N. v. Reich, W. Van Sark, E. Alsema, R. Lof, R. Schropp, W. Sinke, and W. Turkenburg, "Crystalline silicon cell performance at low light intensities," *Solar Energy Materials and Solar Cells*, vol. 93, no. 9, pp. 1471–1481, 2009.

[48] D. Moore, A. Wilson, U. S. D. of Energy, and J. P. L. (U.S.), *Photovoltaic solar panel resistance to simulated hail*. DOE/JPL ; 1012-78/6, Department of Energy, 1978.

[49] F. Liu, L. Jiang, and S. Yang, "Ultra-violet degradation behavior of polymeric backsheets for photovoltaic modules," *Solar Energy*, vol. 108, pp. 88 – 100, 2014.

[50] T. J. Silverman, L. Mansfield, I. Repins, and S. Kurtz, "Damage in monolithic thin-film photovoltaic modules due to partial shade," *IEEE Journal of Photovoltaics*, vol. 6, pp. 1333–1338, Sept 2016.

[51] S. Dongaonkar, C. Deline, and M. A. Alam, "Performance and reliability implications of two-dimensional shading in monolithic thin-film photovoltaic modules," *IEEE Journal of Photovoltaics*, vol. 3, pp. 1367–1375, Oct 2013.

[52] *2DO.3.4 Single Side Versus Double Side Illumination Method IV Measurements for Several Types of Bifacial PV Modules*, 27th European Photovoltaic Solar Energy Conference and Exhibition, Sept. 27 2012.

[53] J. Lindroos and H. Savin, "Review of light-induced degradation in crystalline silicon solar cells," *Solar Energy Materials and Solar Cells*, vol. 147, pp. 115 – 126, 2016.

[54] Y. Jiang, H. Shen, T. Pu, C. Zheng, Q. Tang, K. Gao, J. Wu, C. Rui, Y. Li, and Y. Liu, "High efficiency multi-crystalline silicon solar cell with inverted pyramid nanostructure," *Solar Energy*, vol. 142, pp. 91 – 96, 2017.

[55] G. Bauer, "Absolutwerte der optischen absorptionskonstanten von alkalihalogenidkristallen im gebiet ihrer ultravioletten eigenfrequenzen," *Annalen der Physik*, vol. 411, pp. 434 – 464, Jan-01-1934 1934.

[56] B. Dale and H. Rudenberg, "High efficiency silicon solar cells," in *Proceedings of the 14th Annual Power Sources Conference*, p. 22, U.S. Army Signal Research and Development Lab, U.S. Army Signal Research and Development Lab, 1960 1960. ¡br /¿.

[57] "Iec 60904 photovoltaic devices - part 9: Solar simulator performance requirements," 2007.

[58] "Iec 60904 photovoltaic devices part 3: Measurement principles for terrestrial photovoltaic (pv) solar devices with reference spectral irradiance data," 2008.

[59] B. Van Aken, L. A G Okel, J. Liu, S. Luxembourg, and J. Roosmalen, "White bifacial modules improved stc performance combined with bifacial energy yield," 06 2016.